residues responsible for the enzyme activity. The amino acid substitution is supposed to affect Hex A activity directly and to increase the apparent Km value for a substrate. The apparent Km value of this mutant was estimated to be 30 times higher than that in controls [24]. The R178H mutation has been identified in patients with B1-Variant GM2 gangliosidosis [25-29]. This variant form is known to be an unusual biochemical phenotype, and B1-Variant patients exhibit both Hex A and Hex B activities, as determined with 4-methylumbelliferyl *N*-acetyl-β-D-gluco-saminide (4-MUG), but the mutant Hex A cannot hydrolyze an artificial substrate, 4-methylumbelliferyl 6-sulfo-*N*-acetyl-β-D-glucosaminide (4-MUGS) [19,20]. Brown *et al.* [30] expressed a mutant Hex B with this mutation in COS cells, and confirmed that the mutant enzyme was catalytically inactive, although processing and stability were not affected. These data suggest that the R178H mutation causes a small conformational change inside the active site pocket.

The R504C/H mutations result in disruption of the interaction between the α- and β-subunits in Hex A as an αβ heterodimer. The R504 residue is located in the extrahelix in domain II. This amino acid residue points outside of the extrahelix and is exposed in the monomer. R504 in the α-subunit is thought to bind directly with the D494 residue in the β-subunit at the dimer interface in the αβ heterodimer. In the ββ homodimer, R501, which corresponds to R504 in the α-subunit, binds directly with D494 at the dimer interface. Substitution of R504 to C or H is deduced to cause disruption of the essential binding for dimerization. Paw *et al.* reported that cultured fibroblasts from a patient with R504H synthesized an α-subunit precursor but that the mutant α-subunit failed to associate with the β-subunit to form an active αβ heterodimer [31]. They also reported that R504C gave rise to a mutant α-subunit with the same biochemical defects as those in the case of R504H [32]. The expressed products were each secreted as an α-subunit monomer rather than a dimer of α-subunits. These biochemical results are consistent with the deduced structural information.

Mutations including R170W, W420C, C458Y, L484P and R499C/H were deduced to affect structural stability. The R170 and L484 residues are located in the region of domain II facing domain I, and they are adjacent to each other in the three-dimensional structure. The R170 residue forms hydrogen bonds with E141 in domain I. These hydrogen bonds are thought to contribute to stabilization of domains I and II. R170W is deduced to have a significant destabilizing effect on the domain interface. For the L484P mutation, introduction of P into the α-helix adjacent to domain I may destabilize it.

The W420 and C458 residues are located on the barrel structure enclosing the active site pocket. In contrast with R178H, the structural change caused by W420C and C458Y is large and they might destabilize the core barrel structure of domain II as well as the active site pocket. An expression study showed that the W420C mutation failed to give any catalytic activity with either a sulfated or nonsulfated substrate.

The R499 residue is present on the same extrahelix as R504. But R499 points inside the molecule between domain I and the barrel structure, and is thought to form hydrogen bonds with residues in domain I and the barrel structure. The R499 residue must be one of the important residues stabilizing the two domains. The R499C/H mutations are deduced to cause a loss of stability in this region, although the structural defects are moderate, and not to affect the active site. In cells from patients with R499C/H, residual Hex A activity was detected, and they clinically exhibited the late-onset moderate form of the disease.

3. Structural Defect in Sandhoff Disease

The positions of missense mutations causing Sandhoff disease (R505Q and C534Y) have been mapped in the wild-type structure of Hex B (ββ homodimer), as shown in Fig. **2**.

Among the mutations, C534Y has been identified in a patient with the early-onset severe form of the disease [33], and R505Q in a patient with the late-onset moderate one [34]. The C534 residue is located in the extrahelix between domain I and the barrel structure, and forms a disulfide bond with C551. Substitution of C534 to Y can cause disruption of the disulfide bond, which results in a large conformational change of the extrahelix stabilizing domains I and II. Furthermore, it may affect the dimerization, because the C551 residue is located at the dimer interface [35]. Western blot analysis showed a deficiency of the mature β-subunit and a reduction of the amount of the mature α-subunit [35]. These data suggest that C534Y causes a structurally unstable change in the β-subunit and secondary degradation of the α-subunit resulting from a failure to associate with the β-subunit.

R505Q results in a conformational change of the surface region, although it does not affect the active site. The conformational change caused by R505Q is smaller than that by C534Y. The expressed β-subunit with R505Q is partly processed to the mature form, and shows residual enzyme activity [35].

The structural defects well reflect biochemical and phenotypic abnormalities in the disease. Thus, dysfunctional and destabilizing defects in Hex α- and β-subunits result in Tay-Sachs disease and Sandhoff disease, respectively, and it is thought that enzyme replacement therapies for these diseases will be effective for improvement of the disorders, if the enzyme can be incorporated into neuronal cells.

PRODUCTION OF ENZYMES FOR ENZYME REPLACEMENT THERAPY

As described above, patients with lysosomal diseases accumulate substances to be degraded due to the absence of the enzymes responsible for their hydrolysis in lysosomes. Enzyme replacement therapy, which means administration of the responsible enzyme to the patients, was proposed by de Duve in 1964 [36]. However, large amounts of enzyme proteins are required for enzyme replacement. Enzyme replacement therapy for lysosomal diseases became a reality in early 1990s, when purified glucocerebrosidase derived from human placenta could be targeted to reticuloendothelial tissues, and its safety and effectiveness were demonstrated in Gaucher disease [37]. Now, some recombinant enzymes for lysosomal diseases, such as Gaucher disease [8,9], Fabry disease [10-13], MPS I [14], Pompe disease [15,16], and MPS VI [17], are available, and clinical trials with recombinant enzymes are ongoing for many lysosomal diseases (Table **2**). These recombinant enzymes have been produced in

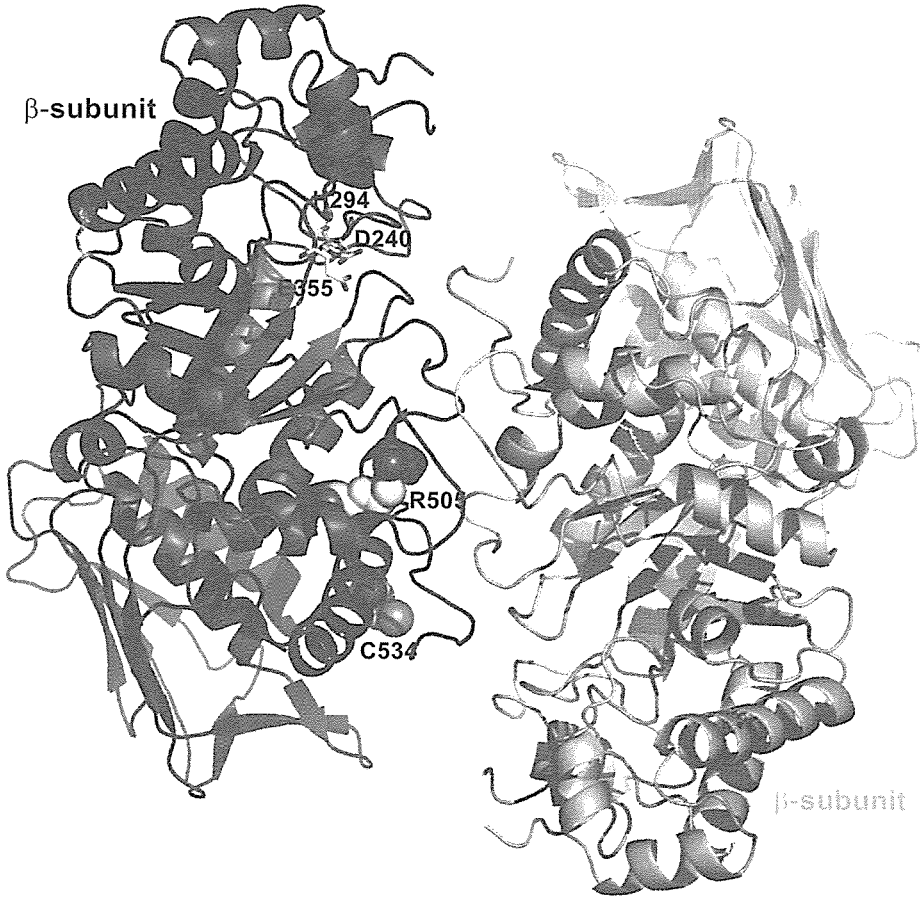

Fig. (2). Three-dimensional structure of human Hex B and residues involved in amino acid substitutions in the β-subunit.
The structure of Hex B (ββ homodimer) is shown. Residues involved in the catalytic triad (D240, H294 and E355) are presented as ball-and-sticks models. Residues involved in amino acid substitutions in the β-subunit (R505 and C534) are presented as space-filling models.

mammalian cells. Many lysosomal enzymes are glycoproteins, and mannose 6-phosphate (M6P) residues at the non-reducing ends of the sugar chains are required for efficient incorporation of the lysosomal enzymes into cells, although mannose residues are essential for incorporation of glucocerebrosidase into reticuloendothelial cells, which are the target cells in Gaucher disease. Lysosomal matrix enzymes are synthesized in rough endoplasmic reticulum and are modified by the addition of high-mannose oligosaccharides. These oligosaccharides are then subjected to the trimming reactions, and the nascent glycoproteins are transferred to the Golgi apparatus, where further modification including addition of M6P recognition maker and binding to M6P receptor occur, and subsequently are transported to endosomes/lysosomes. In some type of cells including fibroblasts, lysosomal enzymes may be transported from the extracellular milieu to lysosomes through M6P receptor-mediated endocytosis [38].

For example, for Fabry disease, two different human α-galactosidases are available: one from human fibroblasts (agalsidase alpha) [10,11] and one from CHO cells (agalsidase beta) [12,13]. Lee *et al.* reported biological and pharmacological comparison of these enzyme preparations [39]. Although the specific activity, *V*max and *K*m toward two different artificial substrates were almost the same for the two enzymes, agalsidase beta showed faster mobility on isoelectric focusing due to the modification of sialic acids on the sugar chains. They exhibited the same *N*-terminal amino acid sequences and *C*-terminal heterogeneity with truncated species lacking either one or two *C*-terminal amino acid residues. However, the predominant molecular species of agalsidase alpha lacked the *C*-terminal leucine, whereas the predominant species of agalsidase beta had the full-length sequence. The most significant difference between them was the pattern of modification of the sugar chains. Monosaccharide analysis indicated that the sialic acid/galactose ratio of agalsidase alpha (0.56) was lower than that of agalsidase beta (0.88), suggesting that the former had more asialo-complex type sugar chains than the latter. This may be due to the differences in host cells and cell culture conditions, and the characteristics of sugar chains should influence the clearance and biodistribution of the enzymes in the whole body. An additional difference in glycosylation between the two enzymes was the amount of M6P residues present on oligomannose side chains. Agalsidase beta had a significantly higher level of M6P (3.1 mol/dimer protein) on a molar basis than agalsidase alpha (1.8 mol/dimer protein). Human α-galactosidase contains three potential *N*-linked glycosylation sites per monomer. The M6P residues are responsible for the incorporation of the enzyme into lysosomes in the cell, because M6P receptors are located on the plasma membrane and play a role in endocytotic trafficking to the endosomes/lysosomes. Phosphorylated oligomannose type sugar chains

were attached to N192 and N215 in both enzymes. However, the amounts of phosphorylated sugar chains of agalsidase beta (72% and 91%) were much higher than those of agalsidase alpha (33% and 61%) for N192 and N215, respectively. These results well correlated with the ability of enzyme binding to the receptors and with that of cellular uptake. When the receptor binding was evaluated by means of surface plasmon resonance analysis to examine the interaction of α-galactosidase with immobilized M6P receptors, agalsidase beta bound to the receptors more than agalsidase alpha did. Cell uptake studies also indicated that the improved binding to the M6P receptors was correlated with the enhanced uptake of agalsidase beta into Fabry fibroblasts. The biodistribution data suggested that the majority of the injected dose was recovered in the liver, however, approximately twice as much agalsidase beta was detected in the kidneys, heart and spleen, compared to agalsidase alpha. These results indicated that the sugar moieties, including the monosaccharide composition, attachment sites and structures of the sugar chains, of the enzymes can influence the effect of enzyme replacement therapy for lysosomal diseases.

Since these recombinant enzymes are produced in mammalian cells, the production of recombinant enzymes is very expensive and careful monitoring for viral infection is essential. Therefore, alternative host cells are required to express an active enzyme at low cost in the near future. *Escherichia coli* [40] and insect cells [41] were used as alternative hosts for producing a recombinant α-galactosidase in early research attempts. However, the recombinant enzyme from *Escherichia coli* was not active and contained no sugar chains. More recently, methylotrophic yeast *Pichia pastoris* was used as a host to produce the α-galactosidase [42]. The expression level of α-galactosidase in this host was considerable (~ 30 mg/L) and the uptake by Fabry fibroblasts was almost the same as that by insect cells; however, the *N*-linked sugar chains of this glycoprotein have not been analyzed carefully and may not have M6P residues at the non-reducing ends. Moreover, it has been reported that *Pichia pastoris* produces a β-mannoside linkage in the associated mannan, which is antigenic for humans [43].

Chiba *et al.* have produced a recombinant α-galactosidase from yeast *Saccharomyces cerevisiae* cells [44]. In order to produce therapeutically effective glycoproteins for lysosomal diseases, the host strain should attach non-antigenic and highly phosphorylated sugar chains to enzyme proteins. Since *Saccharomyces cerevisiae* sometimes produces antigenic hypermannosylated sugar chains, Jigami and co-workers earlier developed a *Saccharomyces cerevisiae* YS132-8B strain that lacked three genes (*OCH1, MNN1,* and *MNN4*) responsible for the biosynthesis of the outer chains of yeast mannan [45,46]. However, since this strain lacked the ability of mannosylphosphorylation, Chiba *et al.* constructed a new disruptant, the HPY21G strain, with KK4 background to delete both *OCH1*, which encodes the initial α-1,6-mannosyltransferase, and *MNN1*, which encodes the terminal α-1,3-mannosyltransferase [44]. It has been reported that the *MNN4* gene encodes a positive regulator of the Mnn6 protein, which transfers mannose phosphate residues to *N*- and *O*-linked sugar chains [46]. The KK4 strain exhibited a higher level of mannosylphosphorylated cell surface than the other strains tested did. As the promoter region of the *MNN4* gene of the *Saccharomyces cerevisiae* KK4 strain had a mutation, the Mnn4 protein was produced constitutively by the KK4 strain. The recombinant α-galactosidase from the *Saccharomyces cerevisiae* HPY21G strain exhibited similar specific activity to that from insect cells, and its apparent molecular mass was a little bit smaller than that of α-galactosidase from mammalian cells. The α-galactosidase contained not only neutral-type sugar chains but also mono- and bis-phosphorylated acidic-type ones. The ratio of non-phosphorylated and phosphorylated sugars of the α-galactosidase was almost 1:2, suggesting that the constitutive expression of *MNN4* in the HPY21G strain may contribute to the increase in the level of phosphorylation of sugar chains of the recombinant α-galactosidase. Monosaccharide composition analysis also showed that the yeast-derived α-galactosidase contained a higher level of M6P (3.8 mol/dimer protein) on a molar basis [44].

Tong *et al.* showed that an uncovered M6P residue was important for the α-galactosidase to exhibit high affinity to the M6P receptor, because with a covered phosphate residue there was no effective binding with the receptor [47]. Since mannose residues covered the M6P residues in *Saccharomyces cerevisiae*, the terminal mannose residues attached through phosphodiester linkages should be removed. Chiba *et al.* have found, on screening, a new bacterium that produces an effective α-mannosidase that digests 'covered' mannose residues on the glycoprotein [44]. The bacterium was determined to be a *Cellulomonas* species. Treatment of the recombinant α-galactosidase with the *Cellulomonas* species α-mannosidase caused exposure of the M6P residues, which was confirmed by structural analysis of the sugar chains by high performance liquid chromatography and M6P receptor binding assaying. Uptake of the recombinant α-galactosidase by cultured Fabry fibroblasts was investigated. The enzyme activity in Fabry cells increased in response to the addition of the treated α-galactosidase and reached a normal level with a concentration of only 0.5 μg/ml in the culture medium. The uptake of the treated α-galactosidase was apparently inhibited by the addition of 5 mM M6P, suggesting that the uptake of the treated α-galactosidase largely depended on the M6P receptor. The effect of the incorporated α-galactosidase on the degradation of ceramide trihexoside accumulated in Fabry fibroblasts was also investigated. After cells had been treated with α-galactosidase for 18 hours, it was likely that the incorporated α-galactosidase was co-localized with ceramide trihexoside and the incorporated α-galactosidase degraded ceramide trihexoside accumulated in the Fabry cells [44].

Such production technology involving a yeast will be useful for producing lysosomal enzymes more economically than with the currently used technology. Efforts are being focused on developing a M6P type glycoprotein production system with a methylotrophic yeast *Ogataea minuta* and on trying to express other lysosomal enzymes including Hex A. The Hex A produced in *Ogataea minuta* exhibits catalytic activities toward synthetic substrates and native substrates under the conditions with a detergent [48].

BRAIN-SPECIFIC DELIVERY OF MEDICINES

To develop effective therapies for lysosomal diseases associated with neurological disorders, a brain-specific delivery system for lysosomal enzymes or their genes is required.

Microglia, macrophage-like cells in the brain, are multifunctional cells; they play important roles in the development, differentiation and maintenance of neuronal cells *via* their phagocytic activity and production of enzymes, cytokines and trophic factors [49]. Although activated microglia show similar phenotypes to macrophages in isolated conditions, they appear to exhibit different phenotypes from those of macrophages *in vivo* and *in vitro* [50-58]. Sawada *et al.* found that when intra-arterially injected into rats, isolated microglia exhibited higher affinity for and migrating activity toward the brain than macrophages did. Since intra-arterially injected microglia, which were labeled with fluorescent dye microparticles through their phagocytic activity, migrated specifically into the brain but were rarely found in the liver, this system could be used as a brain-specific delivery system for medicines or other bioactive materials, such as proteins or genes.

To investigate the possibility that microglia can deliver a gene of interest to the brain without any effect on other organs, a β-galactosidase gene expression vector was transfected into purified microglia from primary mixed brain cultures or Ra2 cells, immortalized microglial clone cells, the microglia then being injected into a vertebral artery in rats. For identification of these exogenous cells within the brain, the cells were tagged with a fluorescent dye specific for phagocytic cells, PKH26 [59,60]. PKH26 stained microglia efficiently; the purified microglia were stained an intensity of at least two-orders higher than the purified astrocytes. Forty-eight hours after the purified microglia had been injected intra-arterially, many fluorescent cells were observed in a brain section from a rat. A small portion of the fluorescent cells was observed in the brain capillaries, attached to the capillary walls. Two hours after the injection, migration of microglia into the brain parenchyma was observed. Exogenous fluorescently labeled microglia were observed to have adhered to a vessel in the medulla of the brain. Some microglia crossed the vessel wall and entered the parenchyma. Similar results were obtained with Ra2 cells. When a frozen brain section was stained with X gal as a substrate for exogenously introduced β-galactosidase, many lacZ-positive cells were observed in the brains of rats at 48 hours after Ra2 cells, which had been transfected with a lacZ-gene expression vector, had been injected intra-arterially. Similar results were obtained with purified microglia. Therefore, intra-arterially injected microglia and Ra2 cells can migrate to the brain, and can express the genes transfected *in vitro* and translate them into biologically active proteins in the brain.

The specificity of Ra2 cell migration was determined by measuring β-galactosidase activity in the brain and other tissues. Using a highly sensitive detection method for β-galactosidase activity involving a chemiluminescent substrate, Sawada *et al.* could detect β-galactosidase activity in frozen sections of the brain and other tissues. β-Galactosidase activity in tissues at 48 hours following the intra-arterial injection of Ra2 cells was highest in the brain, i.e., over 30-fold that in the liver and spleen, and was not detected in lung sections. The results indicated that most of the injected Ra2 cells migrated to the brain. On the other hand, purified macrophages migrated to the liver but were not found in the brain of normal rats [61]. The data indicate that microglia have characteristics differing from those of macrophages; the former exhibit specific affinity for and migrating activity toward the brain. The stability of gene expression in the brain was determined by measuring β-galactosidase activity in brain sections at 2, 9, 16 and 23 days after intra-arterial Ra2 cell injection. β-Galactosidase activity in brain sections was highest on the 2nd day and later gradually decreased. On the 23rd day the β-galactosidase activity was about half that on the 2nd day; the product of the transferred gene was still active. Twenty-three days after the injection, fluorescent Ra2 cells were still present in brain sections in similar numbers to as on day 2, although the fluorescence intensity of Ra2 cells was much weaker than that in the day 2 brain sections. Therefore, the decrease in β-galactosidase activity seemed to be due to a decrease in expression of the lacZ gene in Ra2 cells because it was transiently transfected. This means that if Ra2 cells that express the gene permanently are injected, genes of interest can be expressed in the brain for more than 20 days.

Many types of methods and techniques for *in vivo* gene transfer have been developed, some of which have already been applied in clinical trials. The retroviral system, the most widely accepted gene transfer method to date, allows highly efficient integration, providing the potential for permanent gene expression. However, the system has some major disadvantages, such as the typically low titer, instability of the viral vector obtained, and requirement for target cell division for integration and expression [62]. The adenoviral system allows more efficient gene transfer and greater stability of the virus, however, the difficulties in the control of target cells and re-administration necessitated by the strong antigenicity of the virus are serious problems [63]. *In vivo* electroporation has been demonstrated to allow highly efficient gene transfer into the brain [64]. But all of these methods require a major surgical procedure to transfer cells carrying genes, or the insertion of a stainless steel electrode.

A brain-targeting delivery system involving microglial cell line or related signal peptides which deliver enzyme proteins to the brain will facilitate the development of gene therapies and enzyme replacement therapies for lysosomal diseases including Tay-Sachs disease and Sandhoff disease.

INCORPORATION OF LYSOSOMAL ENZYMES IN TO CELLS

Itoh *et al.* established Chinese hamster ovary cell lines that simultaneously express the human *HEXA* and *HEXB* genes as well as the corresponding murine genes, *Hexa* and *Hexb*, respectively. Mice have the same gene organization as man, i.e., *Hexa* encoding the α-subunit on chromosome 9 and *Hexb* encoding the β-subunit on chromosome 13, and have the same Hex isozyme system [19,65,66]. The amino acid sequences deduced from *Hexa* and *Hexb* cDNAs are 55% identical, and each exhibits homology to the human counterpart, 84% and 75%, respectively [65]. Itoh *et al.* revealed the therapeutic effects of recombinant Hex A isozymes on the degradation of natural substrates including GM2 ganglioside and GlcNAc-oligosaccharides accumulated in cultured cells in Tay-Sachs disease and Sandhoff disease.

CHO cell lines CHO-*HEXA/HEXB* and CHO-*Hexa/Hexb*s were established by co-introduction of the human *HEXA* and *HEXB* as well as the murine *Hexa* and *Hexb* genes, and drug resistance to hygromycin and neomycin derivatives (Itakura submitted). Other CHO cell lines, CHO-

HEXA, CHO-*HEXB* and CHO-*Hexb*, independently expressing the *HEXA*, *HEXB* and *Hexb* genes were also isolated as controls, respectively. As shown in Fig. **3A,B**, the intracellular total Hex activities toward the neutral substrate, 4-MUG for CHO-*HEXA/HEXB* and CHO-*Hexa/Hexb* were similar to those for CHO-*HEXB* and CHO-*Hexb*, and 7~12-fold higher than those for the parent CHO and CHO-*HEXA*, while the Hex activity toward the anionic substrate 4-MUGS was significantly increased by 7- and 5.5-fold, respectively, compared to the levels for the control cell lines. As shown in Fig. **3C,D** the CHO-*HEXA/HEXB* and CHO-*Hexa/Hexb* cell lines were also revealed to produce significant levels of Hex activities toward both 4-MUG and 4-MUGS in the conditioned media, although the levels varied among the cell lines.

Fig. **4** presents the results obtained on immunoblotting with anti-human placental Hex A serum. The CHO-*HEXA* and CHO-*HEXB* cell lines produced and secreted the precursor and mature forms of the corresponding α- (lanes hα) and β- (lanes hβ) subunits, respectively, although these bands were not observed for the parental CHO cells (lanes CHO). The CHO-*HEXA/HEXB* cells also expressed and secreted both the precursor and mature forms of the α- and β-subunits (lanes hαhβ). The molecular masses of the mature subunits were calculated to be 53 kDa for the α_m- and 25 kDa for the β_m-subunit, which were smaller than those of the human placental mature subunits (α_m: 55 kDa and β_m: 28 kDa) as standards. At present, it is unknown whether the difference in subunit size is involved in glycosylation, or it is connected with the difference in protein processing between human placenta and CHO cells.

To examine the corrective effects of the conditioned media containing the recombinant Hex isozymes secreted by the CHO-*HEXA/HEXB* and CHO-*Hexa/Hexb* cell lines, they were administered to skin fibroblasts derived from a Sandhoff patient (SD572) and a Tay-Sachs patient (TS218). As shown in Fig. **5A**, the intracellular 4-MUG-degrading activities in the SD572 cells were restored to 80% and 116% of the control value in normal subjects, respectively. The 4-MUGS-degrading activities in the SD572 cells were also significantly increased by 35% and 67%, respectively, as shown in Fig. **5B**. However, the conditioned media from the CHO-*HEXB* and CHO-*Hexb* cell lines did not cause an increase in 4-MUGS-degrading activity, suggesting that the conditioned media from the CHO-*HEXA/HEXB* and CHO-*Hexa/Hexb* cell lines contained not only the Hex B isozyme but also Hex A and/or Hex S, composed of allo-type Hex subunits. Incorporation of the recombinant Hex isozymes was inhibited in the presence of 5 mM M6P in the culture

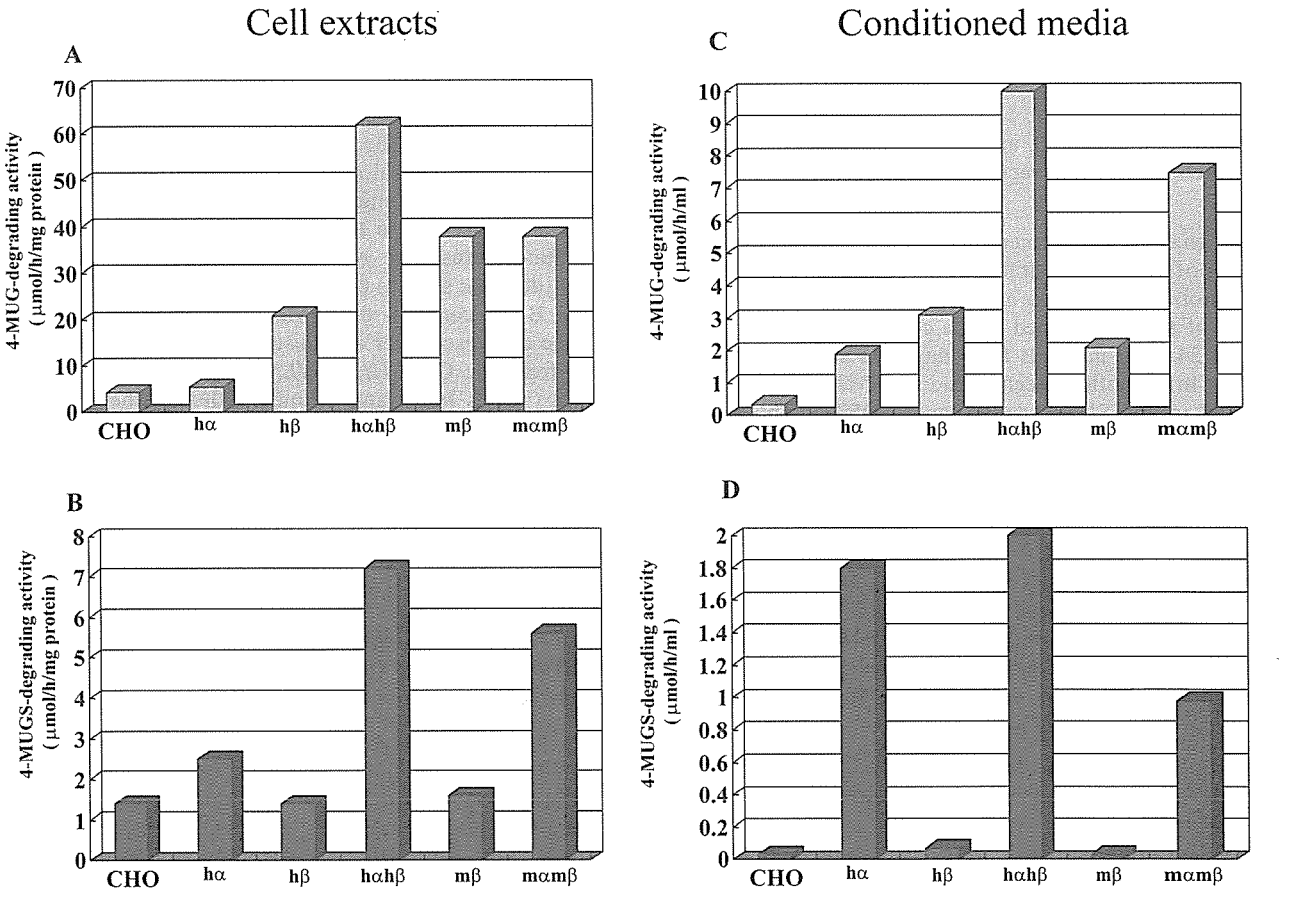

Fig. (3). Expression of Hex subunit genes in stably transformed CHO cell lines.

The intracellular (**A** and **B**) and secreted (**C** and **D**) Hex activities toward synthetic fluorogenic substrates 4-MUG (**A** and **C**) and 4-MUGS (**B** and **D**), respectively, were measured. In panels: CHO, parent CHO; hα, CHO-*HEXA*; hβ, CHO-*HEXB*; hαhβ, CHO-*HEXA/HEXB*; mβ, CHO-*Hexb*; mαmβ, CHO-*Hexa/Hexb*.

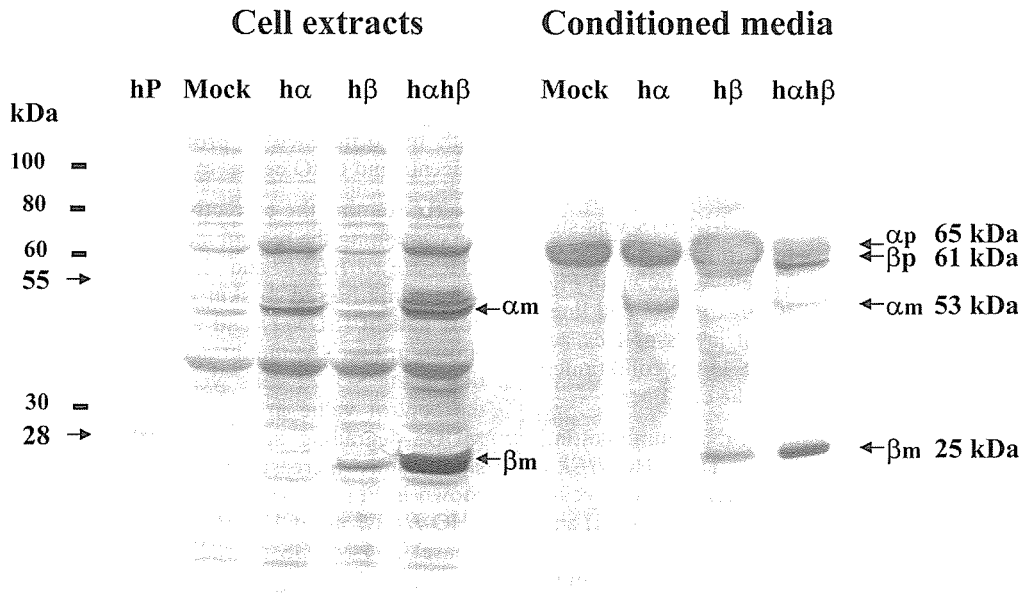

Fig. (4). Immunoblotting of Hex isozymes derived from transformed CHO cell lines stably expressing human Hex α- and β-subunit cDNAs. The isolated clones and conditioned media were harvested, and then aliquots of the cell extracts and conditioned media treated under reducing conditions were subjected to immunoblotting with rabbit anti-human placental Hex A serum, a biotinylated anti-rabbit IgG (Vector, Burlingame, CA), horseradish peroxidase-conjugated egg white avidin (ICN Pharmaceuticals, Inc., Aurora, OH), and chromogenic substrates (NBT and BCIP; GIBCO/LifeTech). In panels: hP, human placental Hex; Mock, parent CHO; hα, CHO-*HEXA*; hβ, CHO-*HEXB*; hαhβ, CHO-*HEXA/HEXB*. The molecular masses (kDa) of biotinylated standards (Cell Signaling Technology, Inc., Beverly, MA) are indicated. Arrows indicate the Hex α-subunit precursor (α_p), β-subunit precursor (β_p), mature α-subunit (α_m), and mature β-subunit (β_m).

medium (open columns), indicating that these Hex isozymes were taken up *via* M6P receptor on the surface of skin fibroblasts.

The enzyme replacement effect on the intracellular degradation of natural substrates accumulated in Sandhoff disease fibroblasts was also analyzed after continuous administration of the conditioned media containing the enzyme activity at 24-hour intervals for 3 days. As shown in Fig. **5C**, granular immunofluorescence due to GM2 ganglioside was observed in the SD572 cells (panel SD572). The accumulated fluorescence due to GM2 ganglioside disappeared after administration of the conditioned media from the CHO-*HEXA/HEXB* and CHO-*Hexa/Hexb* cell lines (panels hαhβ and mαmβ) but not of the conditioned media from the parent CHO cells (panel Mock). The fluorescence due to GlcNAc-oligosaccharides also decreased after the addition of the conditioned media from the CHO-*HEXA/HEXB*, and CHO-*Hexa/Hexb* cell lines, and even the mock one, suggesting that the accumulated GlcNAc-oligosaccharides were easily degraded by the incorporated Hex B derived from man, mouse and hamster (data not shown).

Next, the conditioned media from the CHO-*HEXA/HEXB* and CHO-*Hexa/Hexb* cell lines were administered to Tay-Sachs fibroblasts (TS218). As shown in Fig. **6A**, the 4-MUGS-degrading activities were also restored to 19% and 35% of the control value in normal subjects, which were higher than that (11%) when the conditioned medium from the CHO-*HEXA* cells was added to TS218 cells. The restoration of the intracellular 4-MUGS-degrading activities was also inhibited in the presence of M6P (data not shown).

Fig. **6B** shows the corrective effects of the conditioned media on the natural substrates accumulated in the TS218 cells. The granular immunofluorescence of GM2 ganglioside was also observed in the TS218 cells (panel TS218), while immunofluorescence of GlcNAc-oligosaccharides was absent (data not shown) because of the presence of endogenous Hex B. In contrast, the GM2 ganglioside immunofluorescence decreased after administration of the conditioned media from the CHO-*HEXA/HEXB* and CHO-*Hexa/Hexb* cell lines (panels hαhβ and mαmβ), although the mock conditioned medium could hardly cause a decrease (panel Mock).

These results suggest that the secreted human and murine Hex A derived from the CHO-*HEXA/HEXB* and CHO-*Hexa/Hexb* cell lines were also incorporated *via* M6P receptors to degrade the accumulated GM2 ganglioside in cooperation with GM2 activator protein in fibroblasts in Sandhoff disease and Tay-Sachs disease. Interestingly, the murine Hex A was clearly demonstrated to bind to the human GM2 activator protein to degrade the accumulated GM2 ganglioside in fibroblasts in GM2 gangliosidoses.

There has been recent progress in the development of enzyme replacement therapies for lysosomal diseases *via* cell surface receptors for recombinant lysosomal enzymes with oligosaccharide chains carrying M6P residues, as described above. The application of enzyme replacement therapies with recombinant human Hex isozymes produced by mammalian cells to GM2 gangliosidoses with neurological manifestations is also expected because they have oligosaccharides carrying M6P residues, although the disadvantage of the blood-brain barrier for enzyme replacement therapy still remains. Martino *et al.* reported the difficulty in cross-

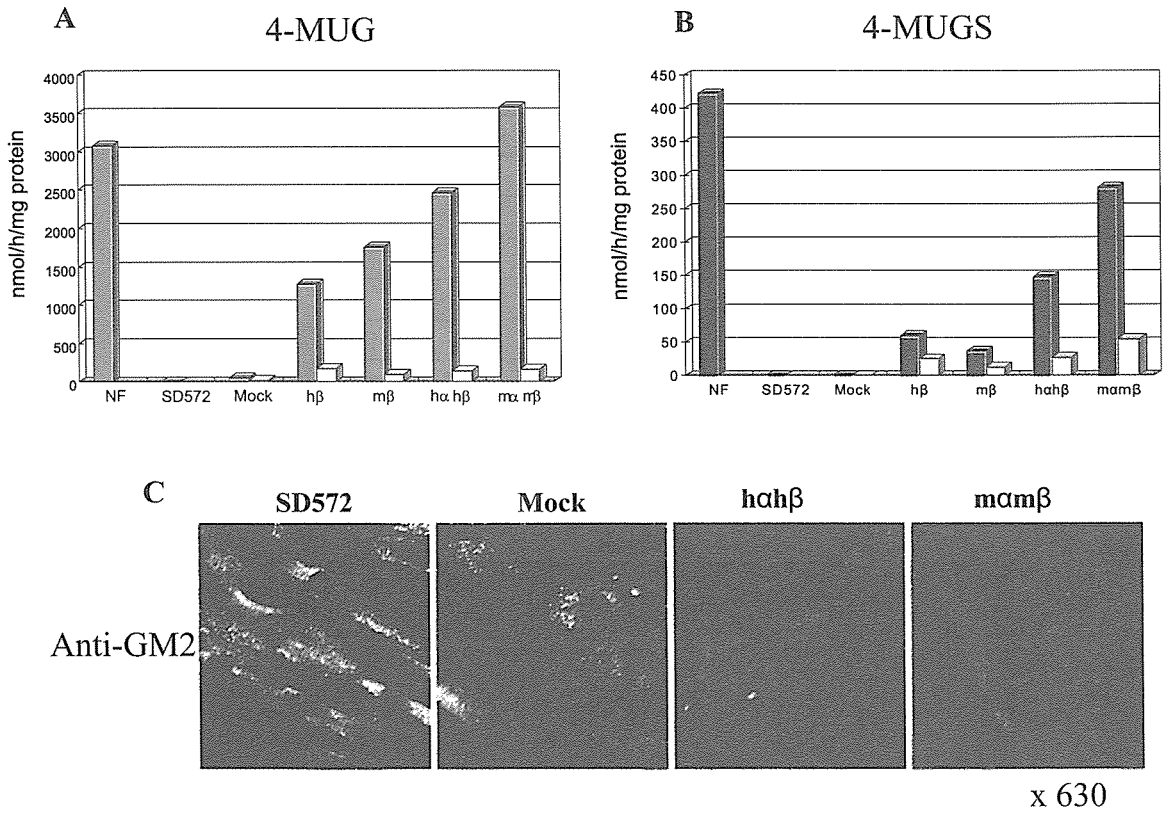

Fig. (5). Corrective effect of the recombinant Hex A on the accumulated natural substrates in Sandhoff fibroblasts.

(**A** and **B**) Concentrated conditioned media containing a definite level of 4-MUG-degrading activity (up to 1 mmol/h) were added repeatedly to the culture medium of Sandhoff fibroblasts (SD572; 1~2 x 10^5 cells/60-mm dish). After 3 days culture, fibroblasts were harvested, and then Hex activities toward synthetic 4-MUG (**A**) and 4-MUGS (**B**) in the cell extracts were measured. Each bar represents the mean for two independent experiments. Some experiments were performed in the presence of 5 mM M6P (open columns). (**C**) Degradation of intracellular GM2 ganglioside accumulated in Sandhoff fibroblasts (SD572) was evaluated by means of immunofluorescence with anti-GM2 ganglioside serum, and then a fluorescein-conjugated second antibody. Magnification, X 630. In panels: NF, normal fibroblasts; SD572, SD572 without the addition of conditioned medium; Mock, SD572 with the addition of conditioned medium from mock-transformed CHO; hβ, conditioned medium from CHO-*HEXB*; mβ, conditioned medium from CHO-*Hexb*; hαhβ, conditioned medium from CHO-*HEXA/HEXB*; mαmβ, conditioned medium from CHO-*Hexa/Hexb*.

correction in Tay-Sachs cells because recombinant Hex A incorporated into the cells could not efficiently degrade the intralysosomal GM2 ganglioside [67]. However, Itoh *et al.* demonstrated that administration of conditioned media derived from the CHO-*HEXA/HEXB* and CHO-*Hexa/Hexb* cell lines, each containing recombinant human and murine Hex A, respectively, to skin fibroblasts from Tay-Sachs and Sandhoff patients partly restored the intracellular 4-MUGS-degrading activities, and significantly decreased the accumulated GM2 ganglioside and GlcNAc-oligosaccharides. As the glycosylated recombinant Hex A containing M6P residues secreted by the CHO cell lines was revealed to be taken up *via* the cell surface M6P receptor, this specific receptor could be the target molecule for enzyme replacement therapies for Tay-Sachs disease and Sandhoff disease patients.

CONCLUSION

We have described the molecular pathologies of Tay-Sachs disease and Sandhoff disease as models of lysosomal diseases from the protein structural aspect, and have discussed enzyme production, targeting to the brain and incorporation into cells. Improvement of these methods and their combination will facilitate the development of efficient enzyme replacement therapies for lysosomal diseases.

ACKNOWLEDGEMENTS

This work was partly supported by grants from CREST, JST, the Tokyo Metropolitan Government, the Japan Society for the Promotion of Science, the Ministry of Education, Science, Sports and Culture, and the Ministry of Health, Labor and Welfare of Japan.

ABBREVIATIONS

CHO = Chinese hamster ovary

MPS = Mucopolysaccharidosis

Hex = β-Hexosaminidase

GlcNAc = *N*-Acetylglucosamine

GalNAc = *N*-Acetylgalactosamine

M6P = Mannose 6-phosphate

4-MUG = 4-Methylumbelliferyl *N*-acetyl-β-D-glucosaminide

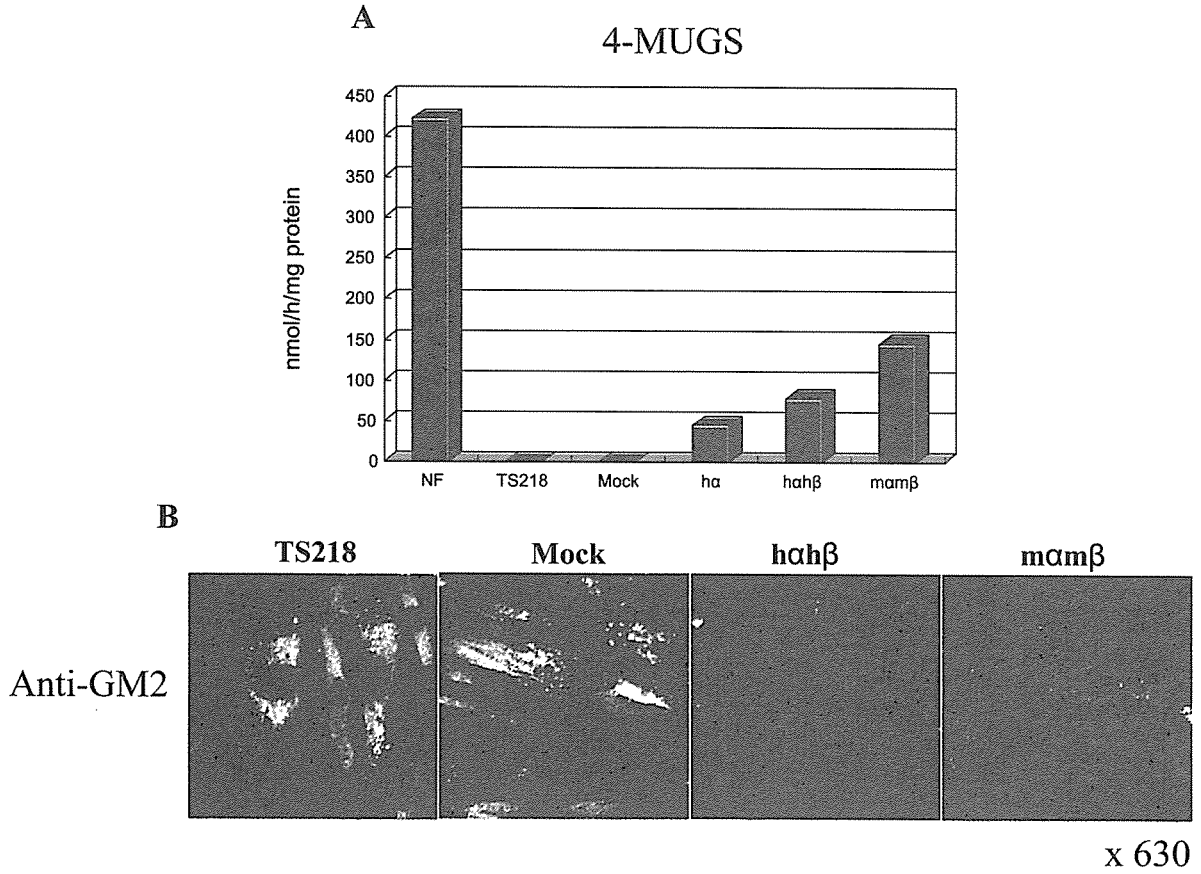

Fig. (6). Corrective effects of the recombinant Hex A on the accumulated natural substrates in Tay-Sachs fibroblasts.

Conditioned media containing a definite amount of 4-MUGS-degrading activity were added repeatedly to the culture medium of Tay-Sachs fibroblasts (TS218; 1~2 x 10^5 cells/60-mm dish). After 3 days culture, fibroblasts were harvested, and then Hex activities toward synthetic 4-MUGS in the cell extracts were measured (***A***). Each bar represents the mean for two independent experiments. (***B***) Degradation of intracellular GM2 ganglioside accumulated in Tay-Sachs fibroblasts (TS218) was evaluated by means of immunofluorescence with anti-GM2 ganglioside serum, and then a fluorescein-conjugated second antibody. Magnification, X 630. In panels: NF, normal fibroblasts; TS218, TS218 with the addition of conditioned medium from mock-transformed CHO; hα, conditioned medium from CHO-*HEXA*; hαhβ, conditioned medium from CHO-*HEXA/HEXB*; mαmβ, conditioned medium from CHO-*Hexa/Hexb*.

4-MUGS = 4-Methylumbelliferyl 6-sulfo-*N*-acetyl-β-D-glucosaminide

GlcNAc-oligosaccharides = Oligosaccharides carrying *N*-acetylglucosamine residues at their non-reducing termini

REFERENCES

[1] Sakuraba, H. http://www.glycoforum.gr.jp/science/word/glycopathology/GD- A05E.html.

[2] Raas-Roothscold, A.; Pankova-Kholmyansky, I.; Kacher, Y.; Futerman, A.H. *Glycoconj. J.* **2004**, *21*, 295.

[3] Guidotti, J.E.; Akli, S.; Casteinau-Ptakhine, L.; Kahn, A.; Poenaru, L. *Hum. Mol. Genet.* **1998**, *7*, 831

[4] Guidotti, J.E.; Haase, G.; Gaillaud, C.; McDonell, N.; Kahn, A.; Poenaru, L. *Hum. Mol. Genet.* **1999**, *8*, 831.

[5] Martino, S.; Cavalieri, C.; Emiliani, C.; Dolcetta, D.; Cusella De Angelis, M.G.; Chigorno, V.; Severini, G.M.; Sandhoff, K.; Bordignon, C.; Sonnino, S.; Orlacchio, A. *Neurochem. Res.* **2002**, *27*, 793.

[6] Jeyakumar, F.; Norflus, M.; Tifft, C.J.; Cortina-Borja, M.; Butters, T.D.; Proia, R.L.; Perry, V.H.; Dwek, R.A.; Platt, F.M. *Blood* **2001**, *97*, 327.

[7] Wada, R., Tifft, C.J.; Proia, R.L. *Proc. Natl. Acad. Sci. USA* **2000**, *97*, 10954.

[8] Grabowski, G.A.; Pastores, G., Brady, R.O.; Barton, N.W. *Pediatr. Res.* **1993**, *33*, 139A.

[9] Grabowski, G.A.; Barton, N.W.; Pastores, G.; Dambrosia, J.M.; Banerjee, T.K.; McKee, M.A.; Parker, C.; Schiffmann, R.; Hill, S.C.; Brady, R.O. *Ann. Intern. Med.* **1995**, *122*, 33.

[10] Schiffmann, R.; Murray, G.J.; Treco, D.; Daniel, P.; Sellos-Moura, M.; Myers, M.; Quirk, J.M.; Zirzow, G.C.; Borowski, M.; Loveday, K.; Anderson, T.; Gillespie, T.; Oliver, K.L.; Jeffries, N.O.; Doo, E.; Liang, T.J.; Kreps, C.; Gunter, K.; Frei, K.; Crutchfield, K.; Selden, R.F.; Brady, R.O. *Proc. Natl. Acad. Sci. USA* **2000**, *97*, 365.

[11] Schiffmann, R.; Kopp, J.B.; Austin, H.A.; Sabnis, S.; Moore, D.F.; Weibel, T.; Balow, J.E.; Brady, R.O. *J. Am. Med. Assoc.* **2001**, *285*, 2743.

[12] Eng, C.M.; Banikazemi, M.; Gordon, R.E.; Goldman, M.; Phelps, R.; Kim, L.; Gass, A.; Winston, J.; Dikman, S.; Fallon, J.T.; Brodie, S.; Stacy, C.B.; Mehta, D.; Parsons, R.; Norton, K.; O'Callaghan, M.; Desnick, R.J. *Am. J. Hum. Genet.* **2001**, *68*, 711.

[13] Eng, CM.; Guffon, N.; Wilcox, W.R.; Germain, D.P.; Lee, P.; Waldek, S.; Caplan, L.; Linthorst G.E.; Desnick, R. J. *N. Engl. J. Med.* **2001**, *345*, 9.

[14] Wraith, J.E.; Clarke, L.A.; Beck, M.; Kolodny, E.H.; Pastores, G.M.; Muenzer, J.; Rapoport, D.M.; Berger, K.I.; Swiedler, S.J.; Kakkis, E.D.; Braakman, T.; Chadbourne, E.; Walton-Bowen, K.; Cox, G.F. *J. Pediatr.* **2004**, *144*, 581.

[15] Klinge, L.; Straub, V.; Neudorf, U.; Schaper, J.; Bosbach, T.; Goerlinger, K.; Wallot, M.; Richards, S.; Voit, T. *Neuromuscul. Disord.* **2005**, *15*, 24.
[16] Van den Hout J.M.P.; Kamphoven, J.H.J.; Winkel, L.P.F.; Arts, W.F.M.; De Klerk, J.B.C.; Loonen, C.B.; Vulto A.G.; Cromme-Dijkhuis, A.; Weisglas-Kuperus, N.; Hop, W.; Van Hirtum, H.; Van Diggelen, O.P.; Boer, M.; Kroos, M.A.; Van Doorn, P.A.; Van der Voort, E.; Sibbles, B.; Van Corven, E.J.J.M.; Brakenhoff, J.P.J.; Van Hove, J.; Smeitink, J.A.M.; de Jong, G.; Reuser, A.J.J.; Van der Ploeg, A.T. *Pediatrics* **2004**, *113*, e448.
[17] Harmatz, P.; Whitley, C.B.; Waber, L.; Pais, R.; Steiner, R.; Plecko, B.; Kaplan, P.; Simon, J.; Butensky, E.; Hopwood, J.J. *J. Pediatr.* **2004**, *144*, 574.
[18] Muenzer, J.; Lamsa, J.C.; Garcia, A.; Dacosta, J.; Garcoa, J.; Treco, D.A. *Acta Paediatr. Suppl.* **2002**, *439*, 98.
[19] Gravel, R.A.; Kaback, M.M.; Proia, R.L.; Sandhoff, K.; Suzuki, K. In *The Metabolic and Molecular Bases of Inherited Disease, 8th* ed., Scriver, C.R.; Beaudet, A.L.; Sly, W.S.; Valle, D., eds.; McGraw-Hill: New York, **2001**; pp. 3827-3876.
[20] Mahuran, D.J. *Biochim, Biophy. Acta* **1999**, *1455*, 105.
[21] Kytzia, H. J.; Sandhoff, K. *J. Biol. Chem.* **1985**, *260*, 7568.
[22] Mark, B.L.; Mahuran, D.J.; Cherney, M.M.; Zhao, D.; Knapp, S.; James, M.N.G. *J. Biol. Chem.* **2003**, *327*, 1093.
[23] Maier, T.; Strator, N.; Schuette, C.G.; Klingenstein, R.; Sandhoff, K. *J. Mol. Biol.* **2003**, *328*, 669.
[24] Matsuzawa, F.; Aikawa, S.; Sakuraba, H.; Tanaka, A.; Ohno, K.; Sugimoto, Y.; Ninomiya, H.; Doi, H. *J. Hum. Genet.* **2003**, *48*, 582.
[25] Tanaka, A.; Pennett, H.H.; Suzuki, K. *Am. J. Hum. Genet.* **1990**, *47*, 567.
[26] Ohno, K.; Suzuki, K. *J. Neurochem.* **1988**, *50*, 316.
[27] Kytzia, H-J.; Hinrichs, U.; Maire, I.; Suzuki, K.; Sandhoff, K. *EMBO J.* **1983**, *2*, 1201.
[28] dos Santos, M.R.; Tanaka, A.; sa Miranda, C.; Ribero, M.G.; Maia, M.; Suzuki, K. *Am. J. Hum. Genet.* **1991**, *49*, 886.
[29] Tanaka, A.; Ohno, K.; Suzuki, K. *Biochem. Biophys. Res. Commun.* **1988**, *156*, 1015.
[30] Brown, C.A.; Neote, K.; Leung, A.; Gravel, R.A.; Mahuran, D.J. *J. Biol. Chem.* **1989**, *264*, 21706.
[31] Paw, B.H.; Moskowitz, S.M.; Uhrhammer, N.; Wright, N.; Kaback, M.M.; Neufeld, E.F. *J. Biol. Chem.* **1990**, *265*, 9452.
[32] Paw, B.H.; Wood, L.C.; Neufeld E.F. *Am. J. Hum. Genet.* **1991**, *48*, 1139.
[33] Kuroki, Y.; Itoh, K.; Nadaoka, Y.; Tanaka, T.; Sakuraba, H. *Biochem. Biophys. Res. Commun.* **1995**, *212*, 564.
[34] Hara, A.; Uyama, E.; Uchino, M.; Shimmoto, M.; Utsumi, K.; Itoh, K.; Kase, R.; Naito, M.; Sugiyama, E.; Taketomi, T.; Sukegawa, K.; Sakuraba, H. *J. Neurol. Sci.* **1998**, *155*, 86.
[35] Sakuraba H.; Matsuzawa, F.; Aikawa, S.; Doi, H.; Kotani, M.; Lin, H.; Ohno, K.; Tanaka, A.; Yamada, H.; Uyama, E. *J. Hum. Genet.* **2002**, *47*, 176.
[36] deDuve, C. *Fed. Proc.* **1964**, *23*, 1045.
[37] Barton, N.W.; Brady, R.O.; Dambrosia, J.M.; Di Bisceglie, A.M.; Doppelt, S.H.; Hill, S.C.; Mankin, H.J.; Murray, G.J.; Parker, R.I.; Argoff, C.E.; Grewal, R.P.; Yu, K-T. *N. Engl. J. Med.* **1991**, *324*, 1464.
[38] Kornfeld, S.; Sly, W.S. In *The Metabolic and Molecular Bases of Inherited Disease, 8th.* ed., Scriver, C.R.; Beaudet, A.L.; Sly, W.S.; Valle, D.S. eds.; McGraw-Hill: New York, **2001**; pp. 3469-3482.
[39] Lee, K.; Jin, X.Y.; Zhang, K.; Copertino, L.; Andrews, L.; Baker-Malcolm, J.; Geagen, L.; Qui, H.W.; Seiger, K.; Barngrover, D.; McPherson, J.M.; Edmunds, T. *Glycobiology* **2003**, *13*, 305.
[40] Hantzopoulos, P.A.; Calhoun, D.H. *Gene* **1987**, *57*, 159.
[41] Coppola, G.; Yan, Y.; Hantzopoulos, P.A.; Segura, E.; Stroh, J.G.; Calhoun, D.H. *Gene* **1994**, *144*, 197.
[42] Chen, Y.; Jin, M.; Egborge, T.; Coppola, G.; Andre, J.; Calhoun, D.H. *Prot. Expr. Purif.* **2000**, *20*, 472.
[43] Vinogradov, E.; Peterson, B.O.; Duus, J.O. *Carbohydr. Res.* **2000**, *325*, 216.
[44] Chiba, Y.; Sakuraba, H.; Kotani, M.; Kase, R.; Kobayashi, K.; Takeuchi, M.; Ogasawara, S.; Maruyama, Y.; Nakajima, T.; Takaoka,Y.; Jigami, Y. *Glycobiology* **2002**, *12*, 821.
[45] Nakanishi-Shindo, Y.; Nakayama, K.; Tanaka, A.; Toda, Y.; Jigami, Y. *J. Biol. Chem.* **1993**, *268*, 26338.
[46] Odani, T.; Shimma, Y.; Tanaka, A.; Jigami, Y. *Glycobiology* **1996**, *6*, 805.
[47] Tong, P.Y.; Gregory, W.; Kornfeld, S. *J. Biol. Chem.* **1989**, *264*, 7962.
[48] Akeboshi, H.; Kasahara, Y.; Tsuji, D.; Tatano, Y.; Itoh, K.; Sakuraba, H.; Chiba, Y.; Jigami, Y. *Seikagaku* **2004**, *76*, 1024.
[49] Sawada, M.; Suzumura, A.; Marunouchi, T. *Int. J. Dev. Neurosci.* **1995**, *13*, 253.
[50] Gehrmann, J.; Matsumoto, Y.; Kreutzberg, G.W. *Brain Res. Rev.* **1995**, *20*, 269.
[51] Kurihara, Y.; Matsumoto, A.; Itakura, H.; Kodama, T. *Curr. Opin. Lipidol.* **1991**, *2*, 295.
[52] Lassmann, H.; Schmied, M.; Vass, K.; Hickey, W.F. *Glia* **1993**, *7*, 19.
[53] Sawada, M.; Suzumura, A.; Yamamoto, H.; Marunouchi, T. *Brain Res.* **1990**, *509*, 119.
[54] Sawada, M.; Suzumura, A.; Marunouchi, T. *Biochem. Biophys. Res. Commun.* **1992**, *189*, 869.
[55] Sawada, M.; Suzumura, A.; Itoh, Y.; Marunouchi, T. *Neurosci. Lett.* **1993**, *155*, 175.
[56] Sawada, M.; Suzumura, A.; Marunouchi, T. *J. Neurochem.* **1995**, *64*, 1973.
[57] Suzumura, A.; Marunouchi, T.; Yamamoto, H. *Brain Res.* **1991**, *545*, 301.
[58] Ziegler-Heitbrock, H.W.L.; Ulevitch, R.J. *Immunol. Today* **1993**, *14*, 121.
[59] Horan, P.K; Slezak, S.E. *Nature* **1989**, *340*, 167.
[60] Melnicoff, M.J.; Horan, P.K.; Breslin, E.W.; Morahan, P.S. *J. Leukoc. Biol.* **1998**, *44*, 367.
[61] Ishihara, S.; Sawada, M.; Chang, L.; Kim, J.M.; Brightman, M. *Exp. Neurol.* **1993**, *124*, 219.
[62] Mulligan, R.C. *Science* **1993**, *260*, 926.
[63] Kozarsky, K.F.; Wilson, J.M. *Curr. Opin. Genet. Dev.* **1993**, *3*, 499.
[64] Nishi, T.; Yoshizato, K.; Yamashiro, S.; Takeshima, H.; Sato, K.; Hamada, K.; Kitamura, I.; Yoshimura, T.; Saya, H.; Kuratsu, J.; Ushio, Y. *Cancer Res.* **1996**, *56*, 1050.
[65] Yamanaka, S.; Johnson, O.N.; Norflus, F.; Boles, D.J.; Proia, R.L. *Genomics* **1994**, *21*, 588.
[66] Wakamatsu, N.; Benoit, G.; Lamhonwah, A.; Zhang, Z.X.; Trasler, J.M.; Raine, B.L.; Gravel, R.A. *Genomics* **1994**, *24*, 110.
[67] Martino, S.; Emiliani, C.; Tancini, B.; Severini, G.M.; Chigorno, V.; Bordignon, C.; Sonnino, S.; Orlacchio, A. *J. Biol. Chem.* **2002**, *277*, 20177.

Received: August 16, 2005 **Accepted: June 2, 2006**

Neuroscience 142 (2006) 87–96

THE INTRA-ARTERIAL INJECTION OF MICROGLIA PROTECTS HIPPOCAMPAL CA1 NEURONS AGAINST GLOBAL ISCHEMIA-INDUCED FUNCTIONAL DEFICITS IN RATS

Y. HAYASHI,[a] Y. TOMIMATSU,[a] H. SUZUKI,[b] J. YAMADA,[a] Z. WU,[a] H. YAO,[c] Y. KAGAMIISHI,[d] N. TATEISHI,[d] M. SAWADA[b] AND H. NAKANISHI[a]*

[a]*Laboratory of Oral Aging Science, Faculty of Dental Sciences, Kyushu University, Fukuoka 812-8582, Japan*

[b]*Department of Brain Life Science, Research Institute of Environmental Medicine, Nagoya University, Nagoya 464-8601, Japan*

[c]*Laboratory for Neurochemistry, Hizen National Hospital, Saga 342-0192, Japan*

[d]*Minase Research Laboratories, Ono Pharmaceutical Co., Ltd., Osaka 618-8585, Japan*

Abstract—In the present study, we have attempted to elucidate the effects of the intra-arterial injection of microglia on the global ischemia-induced functional and morphological deficits of hippocampal CA1 neurons. When PKH26-labeled immortalized microglial cells, GMIR1, were injected into the subclavian artery, these exogenous microglia were found to accumulate in the hippocampus at 24 h after ischemia. In hippocampal slices prepared from medium-injected rats subjected to ischemia 48 h earlier, synaptic dysfunctions including a significant reduction of synaptic responses and a marked reduction of long-term potentiation (LTP) of the CA3–CA1 Schaffer collateral synapses were observed. At this stage, however, neither significant neuronal degeneration nor gliosis was observed in the hippocampus. At 96 h after ischemia, there was a total loss of the synaptic activity and a marked neuronal death in the CA1 subfield. In contrast, the basal synaptic transmission and LTP of the CA3–CA1 synapses were well preserved after ischemia in the slices prepared from the microglia-injected animals. We also found the microglial-conditioned medium (MCM) to significantly increase the frequency of the spontaneous postsynaptic currents of CA1 neurons without affecting the amplitude, thus indicating that MCM increased the provability of the neurotransmitter release. The protective effect of the intra-arterial injected microglia against the ischemia-induced neuronal degeneration in the hippocampus was substantiated by immunohistochemical and immunoblot analyses. Furthermore, the arterial-injected microglia prevented the ischemia-induced decline of the brain-derived neurotrophic factor (BDNF) levels in CA1 neurons. These observations strongly suggest that the arterial-injection of microglia protected CA1 neurons against the ischemia-induced neuronal degeneration. The restoration of the ischemia-induced synaptic deficits and the resultant reduction of the BDNF levels in CA1 neurons, possibly by the release of diffusible factor(s), might thus contribute to the protective effect of the arterial-injection of microglia against ischemia-induced neuronal degeneration.

Key words: microglia, intra-arterial injection, global ischemia, hippocampal CA1 neurons, brain-derived neurotrophic factor, electrophysiology.

In response to pathological conditions including cerebral ischemia, ramified microglia rapidly transform into activated states and accumulate in pathological sites. When neurons are severely injured, the microglia further transform into phagocytic cells. It remains controversial whether the microglia which accumulate at pathological sites are harmful or beneficial. There is growing evidence that the activated microglia are harmful for the injured neurons associated with ischemia, while the inhibition of microglial activation could reduce ischemic brain injury (Lees, 1993). Lipid-soluble tetracyclines, doxycycline and minocycline, have been reported to inhibit microglial activation, while they also have a neuroprotective effect against global brain ischemia (Yrjänheikki et al., 1998). On the other hand, some studies have suggested that microglia might have a beneficial effect on ischemic injured neurons. The proliferation of microglia after ischemia has also been suggested to contribute to the ischemic tolerance (Liu et al., 2001).

The intra-cerebral introduction of microglia is one of the direct approaches to elucidate the role of microglia in the ischemic brain. Recently, Kitamura et al. (2004, 2005) examined the effects of i.c.v.-injected microglia on neurodegeneration induced by the middle cerebral artery occlusion (MCAO) and reperfusion. After MCAO, i.c.v.-injected microglia were found to accumulate in the infracted core in rat brain parenchyma. They performed histological and functional analyses to show a neuroprotective effect of exogenous microglia on neuronal injury induced by MCAO. Unfortunately, i.c.v.-injected microglia may induce several undesirable events such as the entry of blood cells to the ischemic lesions and immunologic responses, which complicate the analysis of the role of microglia. We have previously reported that microglial cell lines as well as primary cultured microglia retain the ability to enter the normal brain from the circulation (Imai et al., 1997; Sawada et al., 1998; Imai et al., 1999). Furthermore, intra-arterial-injected microglia migraded to the ischemic hippocampal CA1 sub-

*Corresponding author. Tel: +81-92-642-6413; fax: +81-92-642-6415.
E-mail address: nakan@dent.kyushu-u.ac.jp (H. Nakanishi).

Abbreviations: BDNF, brain-derived neurotrophic factor; CD, cathepsin D; CLSM, confocal laser-scanning microscope; FCS, fetal calf serum; GFAP, glial fibrillary acidic protein; Iba1, ionized calcium binding adaptor molecule 1; I–O, input–output; LTP, long-term potentiation; MAP2, microtubule-associated protein-2; MCAO, middle cerebral artery occlusion; MCM, microglial-conditioned medium; MEM, minimal essential medium; NeuN, neuronal nuclei; NMDA, *N*-methyl-D-aspartic acid; PBS, phosphate-buffered saline; pEPSP, population excitatory postsynaptic potential; PI, propidium iodide; rCBF, regional cerebral blood flow; SDS, sodium dodecyl sulfate.

0306-4522/06$30.00+0.00 © 2006 IBRO. Published by Elsevier Ltd. All rights reserved.
doi:10.1016/j.neuroscience.2006.06.003

field, one of the most vulnerable neuronal populations against global forebrain ischemia (Imai et al., 1997, 1999). Therefore, the intra-arterial injection of microglia can be a suitable approach to address the question of whether microglia are harmful or beneficial to the ischemic neuronal injury.

In the present study, we have thus utilized this intra-arterial injection system and found that the arterial-injected microglia protected CA1 neurons against the ischemia-induced neuronal degeneration by a combination of electrophysiological and morphological analyses. The arterial-injected microglia ameliorated the ischemia-induced synaptic deficits and the resultant reduction of brain-derived neurotrophic factor (BDNF) levels in CA1 neurons possibly by releasing diffusible factor(s). These effects might contribute to the protective effect of the arterial-injection of microglia against the ischemia-induced neuronal degeneration.

EXPERIMENTAL PROCEDURES

Animals

This study was approved by the Animal Research Committee of the Kyushu University Faculty of Dental Sciences. The study was carried out using male Wistar rats weighing 180–210 g. The rats were housed in group cages under 12-h light/dark conditions and then were given free access to food and water. The experimental procedure was approved by the Animal Research Committee of the Kyushu University Faculty of Dental Sciences, and was conducted in accordance with the guidelines of the U.S. National Institutes of Health on the Care and Use of Laboratory Animals. Every effort was made to minimize the number of animals used and their suffering.

Cell culture

GMIR1, an immortalized microglial clone, was established from a rat primary microglial culture which has been described previously (Morihata et al., 2000; Salimi et al., 2002). GMIR1 cells displayed strong wheat germ agglutinin and IB4-lectin binding and immunoreactivity for antibodies recognizing OX-42 and ED1, indicating that this clone had microglial properties (Salimi et al., 2002). GMIR1 cells were cultured in Petri dishes in Eagle's minimal essential medium (MEM) containing 10% fetal calf serum (FCS), 0.2% glucose, 5 mg/l bovine insulin, pH 7.3 and supplemented with 1 ng/ml granulocyte-macrophage colony stimulating factor (Genzyme, Cambridge, MA, USA) at 37 °C in 5% CO_2. Before injection, the cells were tagged with a lipid-soluble fluorescent dye PKH-26 (Zynaxis, Malvern, PA, USA). PKH26-stained cells were harvested using a rubber policeman in 2 ml of ice-cold phosphate-buffered saline (PBS) which was centrifuged three times.

Preparation of peritoneal macrophages

Macrophages were collected by injecting 20 ml of cold (4 °C) PBS into the peritoneal cavities of male Wistar rats. Peritoneal fluid was withdrawn three times with a 21-gauge needle and a plastic syringe. The cells were kept at 4 °C, centrifuged at 1000×*g* for 5 min, and seeded onto plastic dishes containing MEM with 10% FCS. The non-adherent cells were removed after 2 h and the adherent macrophages were cultured for 24 h in MEM containing 10% FCS, where they were allowed for 1 h at 37 °C in 5% CO_2.

Microglial injection and forebrain ischemia

Male Wistar rats were anesthetized with halothane and the tagged microglial cells (2×10^6 cells in 500 μl of medium) were injected as a bolus over 30 s into the recipient's subclavian artery. In some experiments, microglia fixed with 4% paraformaldehyde or peripheral macrophages (2×10^6 cells in 500 μl of medium) were injected into the recipient's subclavian artery. Four to 7 days after injection, rats were subjected to transient forebrain ischemia by clamping the carotid arteries bilaterally according to the method of Pulsinelli and Brierley (1979). Briefly, the animals were anesthetized with the mixture of ketamine (50 mg/kg) and xylazine (10 mg/kg) and bilateral vertebral arteries were electrocauterized at the level of the first vertebra. On the following day, the common carotid arteries were gently exposed and both arteries were occluded with a vascular clamp for 10 min. The rectal temperature was maintained at 36.5–37.5 °C. The rats that had lost their righting reflexes during the period of ischemia were used as the postischemic group. This procedure induced a total loss of neurons in the hippocampal CA1 subfield of medium-injected rats assessed by Nissl staining and microtubule-associated protein-2 (MAP2)-immunohistochemistry. In a parallel set of experiments, the changes in the regional cerebral blood flow (rCBF) (1 mm posterior and 2–4 mm lateral to the bregma) were continuously monitored with a laser-Doppler flowmeter (ALF 21D, Advance Co. Ltd., Tokyo, Japan). The changes in the rCBF were expressed as a percentage of the average of two to three baseline values. After bilateral carotid occlusion, the rCBF decreased to 19.9% (range: 12.0–25.0%, number of animals=3) and 14.7% (range: 9.1–21.4%, number of animals=4) of the control values in the medium- and microglia-injected animals, respectively. The extents of rCBF reduction after carotid occlusion did not differ between the two groups.

Quantitative analysis of infiltrated cells

PKH26-labeled microglia-injected sham and animals subjected to 10-min of four-vessel occlusion 24 h and 48 h earlier (number of animals=3, each) were anesthetized with sodium pentobarbital (40 mg/kg, i.p.) and killed by intracardiac perfusion with isotonic saline followed by a chilled fixative consisting of 4% paraformaldehyde in 0.2 M PBS (pH 7.4). After perfusion, the brain was removed and further fixed by immersion in the same fixative overnight at 4 °C, and then immersed in 20% sucrose (pH 7.4) for 24 h at 4 °C. Serial parasagittal sections (10 μm thick) of the whole hippocampus were prepared by a cryostat. Three sections were randomly selected from each group. Images of PKH26-positive cells infiltrated in each section were taken as a stack at 1-μm step size along z-direction with a 20× objective by a confocal laser-scanning microscope (CLSM) (LSM510MET, Carl Zeiss, Jena, Germany) (Shimizu et al., 2005).

Electrophysiology

For electrophysiological analyses, postischemic slices were taken from either group subjected to 10-min of four-vessel occlusion 48 h (number of animals=5, each group), 96 h (number of animals=5, each group) and 1 week (number of animals=3) earlier. Sham slices were taken from medium- and microglia-injected animals subjected to identical surgical exposure without vessel occlusion 96 h (number of animals=3, each group) earlier. Animals of both the ischemic and sham groups were decapitated under light ether anesthesia and then were rapidly removed and placed in ice-cold Krebs Ringer solution of the following composition (in mM): NaCl 124.0, KCl 2.5, KH_2PO_4 1.24, $NaHCO_3$ 26.0, $CaCl_2$ 2.4, $MgSO_4$ 1.3 and glucose 10.0. Transverse hippocampal slices (thickness of 400 μm) ranging from 2.0–3.5 mm lateral to the midline were cut with a vibrating microtome (VT 1000S, Leica, Heidelberg, Germany) were used for electrophysiological studies. A single hippocampal slice was placed in an interface-type record-

ing chamber at a constant bath temperature of 32±0.1 °C. Electrical stimulation (intensity 0–40 V, duration 20 μs, frequency 0.3 Hz) was applied to Schaffer collateral afferents through a bipolar stainless steel electrode. The extracellular field potentials were recorded with a glass electrode filled with perfusate and placed on the stratum pyramidal or stratum radiatum of the CA1 subfield. Stimulus-response curves were constructed by using stimulus intensities from 0 to 40 V in increments of 5 V. The responses were subsequently set to a level that gave a slope value 20% of the maximum obtained. Baseline responses were obtained every 30 s. Paired-pulse facilitation was assessed using a succession of paired pulses separated by intervals of 25, 50, 100, 200, and 300 ms. An additional 30 min baseline period was obtained before attempting to induce long-term potentiation (LTP). LTP experiments were performed on transverse hippocampal slices as described previously (Tomimatsu et al., 2002). LTP was induced by tetanus stimulation, consisting of a train of pulses of 1 s duration with a tetanus at 100 Hz, given at the test stimulus intensity.

For whole cell recordings, transverse hippocampal slice (thickness of 400 μm) from male Wistar rats weighing 100–120 g were cut with a vibrating microtome (VT 1000S, Leica) in ice-cold Krebs Ringer solution. The slices were placed in an interface-type chamber at a constant bath temperature of 32±0.1 °C. Whole-cell recordings were obtained from CA1 pyramidal cells using blind patch clamp technique in the whole cell voltage clamp mode (EPC-9, HEKA, Lambrecht, Germany). Patch electrode of 4–7 MΩ from glass (outer diameter 1.5 mm, inner diameter 0.9 mm, WPI) were fabricated on a puller (Model P-97, Sutter Instruments, Novato, CA, USA). For recording spontaneous miniature currents, internal solution was composed of (in mM): $CsMeSO_3H$ 130, TEA-Cl 5, CsCl 5, EGTA 2, Hepes 10, $MgCl_2$ 1, ATP-Mg 4, and pH was adjusted to 7.4 with Tris-base. Series resistance was continuously monitored during recordings. All experiments were filtered at 2 kHz, digitized at 4 kHz and stored on a computer equipped with A/D converter (Power Laboratory). Spontaneous miniature currents were counted and analyzed using the MiniAnalysis program (Synaptosoft, Decatur, GA, USA). Spontaneous events were screened automatically using an amplitude threshold of 15 pA and then visually accepted or rejected based on the rise and decay times. The average values of frequency and amplitude of spontaneous miniature currents during the control period were calculated, and the frequency and amplitude of all the events during MCM application were normalized to these values.

Immunohistochemistry

For immunohistochemistry, animals subjected to 10-min of four-vessel occlusion 48 h (number of animals=3, each group), and 96 h (number of animals=3, each group) earlier were deeply anesthetized with sodium pentobarbital (100 mg/kg, i.p.) and then transcardially perfused with isotonic saline, followed by a chilled fixative consisting of 4% paraformaldehyde in 0.1 M phosphate buffer (pH 7.4). The brain was left *in situ* for 2 h at room temperature and then it was removed from the skull. Small blocks containing the hippocampus separated from the brain were further fixed by immersion in the same fixative overnight, cryoprotected overnight in 30% sucrose in PBS, and were then embedded in an optimal cutting temperature compound (Sakura Finetechnical Co., Ltd., Tokyo, Japan). Floating parasaggital sections (40 μm thick) of the hippocampus were prepared by a cryostat and stained with anti-MAP2 (1:1000) (Chemicon International, Temecula, CA, USA), anti-cathepsin D (CD, 5 μg/ml), anti-CD11b (1:200) (OX42, Serotec, Bichester, UK), anti-glial fibrillary acidic protein (1:1000) (GFAP, Chemicon International) or anti-ionized calcium binding adaptor molecule 1 (1:500) (Iba1, Wako Pure Chemical Industries, Inc., Osaka, Japan) antibodies for 3 days at 4 °C. Antisera to purified rat spleen CD was raised in rabbits and purified by affinity chromatography. After washing with PBS, the sections were incubated with biotinylated anti-goat or anti-horse IgG for 2 h at room temperature. After washing with PBS, the sections were incubated with streptavidin-Alexa 488 (Molecular Probes Inc., Eugene, OR, USA) for 2 h at room temperature. After washing with PBS, the sections were further stained with propidium iodide (PI, 5 μM/ml) (Sigma Chemical Company, St. Louis, MO, USA) for 5 min at room temperature. For double staining, floating sections were incubated with anti-BDNF (1:50) (Santa Cruz Biotechnology, Santa Cruz, CA, USA) and anti-neuronal nuclei (1:200) (NeuN, Chemicon International) antibodies for 3 days at 4 °C. After washing with PBS, the sections were incubated with a mixture of fluorescein isothiocyanate-conjugated donkey anti-rabbit IgG and rhodamine-conjugated donkey anti-mouse IgG for 1 h at room temperature. After several washes with PBS, the sections were mounted in the anti-fading medium Vectashield (Vector Laboratories, Burlingame, CA, USA) and then were examined with the CLSM (LSM510MET, Carl Zeiss). For the quantitative assessment of the immunofluorescence of BDNF, the immunofluorescence intensity was determined as the average pixel intensity in the CA1 subfield of the hippocampus.

Immunoblotting

For immunohistochemical analyses, the dorsal hippocampus was taken from either group subjected to 10-min of four-vessel occlusion 48 h (number of animals=3, each group), and 96 h (number of animals=3, each group) earlier. As the sham sample, the dorsal hippocampus was also taken from the medium- and microglia-injected animals subjected to identical surgical exposure without vessel occlusion 96 h (number of animals=3, each group) earlier. The animals were anesthetized by sodium pentobarbital anesthesia (40 mg/ml, i.p.) and killed by intracardiac perfusion with isotonic saline. The soluble fractions obtained from the hippocampus homogenates by differential centrifugation, as described below, were electrophoresed using sodium dodecyl sulfate (SDS)–polyacrylamide gels. Proteins on SDS gels were transferred electrophoretically at 100 V for 12–15 h from the gel to nitrocellulose membranes and then incubated at 4 °C overnight under gentle agitation with primary antibody against CD or MAP2. After washing, the membranes were incubated with 0.5% horseradish peroxidase–labeled donkey anti-rabbit IgG (Amersham, Buckinghamshire, UK). Subsequently, membrane-bound, HRP-labeled antibodies were detected by an enhanced chemiluminescence detection system kit (Amersham). As a control, the primary antibody was replaced by nonimmune rabbit IgG. The protein bands were scanned and analyzed densitometrically.

Preparation of microglial-conditioned medium (MCM)

Mixed glial cells were prepared from the cerebral cortex of 3-day-old Wistar rats and cultured in Eagle's MEM (Nissui Pharmaceutical Co., Tokyo, Japan) containing 10% fetal bovine serum (HyClone, Logan, UT, USA), 0.2% $NaHCO_3$, 2 mM glutamine, 0.2% glucose, 25 μg/ml insulin, 5000 U/ml penicillin and 5 mg/ml streptomycin according to the methods described previously (Moriguchi et al., 2003). After isolation, microglia were replaced in six-well plates (2×10^6/ml) and maintained in serum-free MEM containing 0.2% $NaHCO_3$, 2 mM glutamine, 0.2% glucose, 25 μg/ml insulin, 5000 U/ml penicillin and 5 mg/ml streptomycin. After 2 days in culture, supernatants were retrieved and filtered by 0.22-μm filter (Millex-GS, Millipore, Billerica, MA, USA) and stored at −80 °C.

Statistical analysis

The experimental values are shown as the mean±S.E. Statistical analyses of the results were evaluated using the Student's *t*-test.

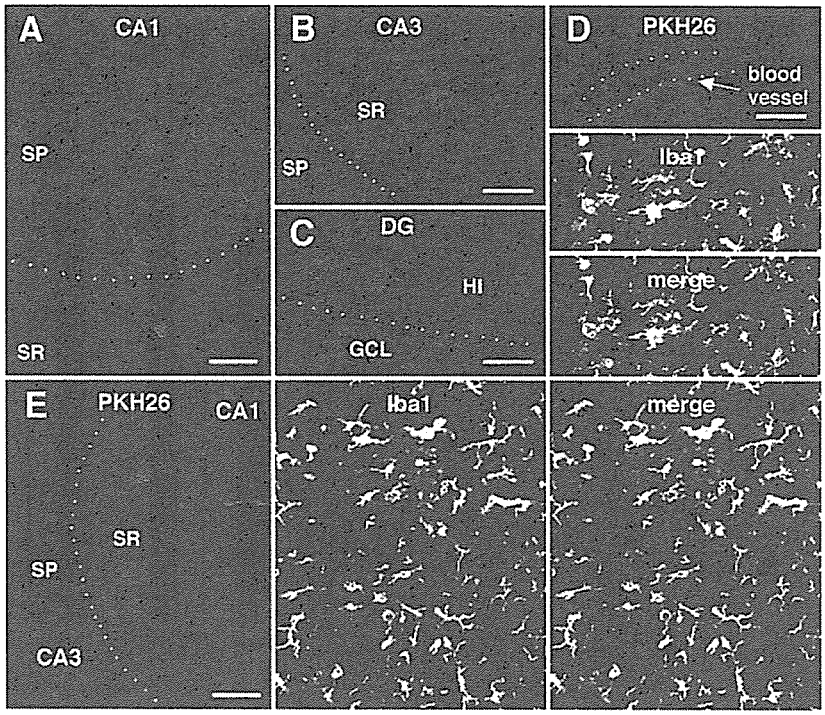

Fig. 1. Infiltration of arterial-injected PKH26-labeled microglia in the hippocampus at 24 after ischemia. (A–C) PKH26-labeled cells distributed in the CA1 subfield (A), the CA3 subfield (B), and the dentate hilus (C). (D, E) Immunofluorescent CLSM images for PKH26 (red) and Iba1 (green) in the CA3 subfield of the hippocampus. The hippocampal sections containing PKH-labeled cells were subjected to an indirect immunofluorescence analysis with anti-Iba1 antibody. Most PKH26-labeled cells were thus found to be positive for Iba1. Scale bars=50 μm (A–D), 80 μm (E).

RESULTS

Infiltration of intra-arterial injected microglia in the post-ischemic brain

In sham animals, PKH26-labeled cells were detected only in the vessels of the various brain regions but not in the brain parenchyma including the hippocampus. In the sections prepared from the animals subjected to the transient ischemia 24 h earlier, round- or oval-shaped PKH26-labeled cells were distributed throughout the hippocampus. In the CA1 subfield, PKH26-labeled cells were mainly detected in the pyramidal cell layer (Fig. 1A). On the other hand, in the CA3 subfield, PKH26-labeled cells were mainly distributed in the dendritic fields (Fig. 1B). PKH26-labeled cells were also scattered in the dentate hilus (Fig. 1C). The mean cell number of PKH26-labeled cells/section (10 μm thickness) in the CA1 and CA3 regions was 15.7±1.0 and 19.3±1.3 (number of sections=14), respectively. The total cell number of PKH26-labeled cells migrated in the hippocampus at 24 h after forebrain ischemia ranged from 1400–1800. When hippocampal sections were immunostained for Iba1, which is specifically expressed in cells of the monocytic lineage including microglia (Imai et al., 1996), PKH26-labeled cells adhered to the blood vessels were observed to be immunostained for Iba1 (Fig. 1D). Some cells resided in the parenchyma close to the blood vessels. As shown in Fig. 1E, most PKH26-labeled cells observed in the parenchyma were also positive for Iba1. In the sections prepared from the animals subjected to ischemia 48 h and 96 h earlier, however, PKH26-labeled cells were rarely detectable in the CA1 subfield.

Protective effects of intra-arterial microglial injection against the ischemia-induced changes in the evoked synaptic responses in the hippocampal CA1 pyramidal cells

Next, we examined the effects of the intra-arterial injection of microglia on the ischemia-induced changes in synaptic responses in hippocampal slices. The field potentials elicited by the stimulation of the CA3–CA1 Schaffer collateral pathway were simultaneously recorded from the somatic (upper traces) and dendritic (lower traces) areas of the hippocampal CA1 subfield prepared from the medium- and microglia-injected animals subjected to the transient ischemia.

In the sham slices of both groups, an upward waveform followed by a single population spike was recorded from the CA1 somatic area of sham slices. When recorded from the dendritic area of the CA1 subfield, the population excitatory postsynaptic potentials (pEPSPs) consisting of a downward waveform with a single positive reflection was observed. No significant difference in the synaptic responses was observed between these two groups (Fig. 2A, D). In the slices prepared from the medium-injected animals subjected to ischemia 48 h earlier, the mean max-

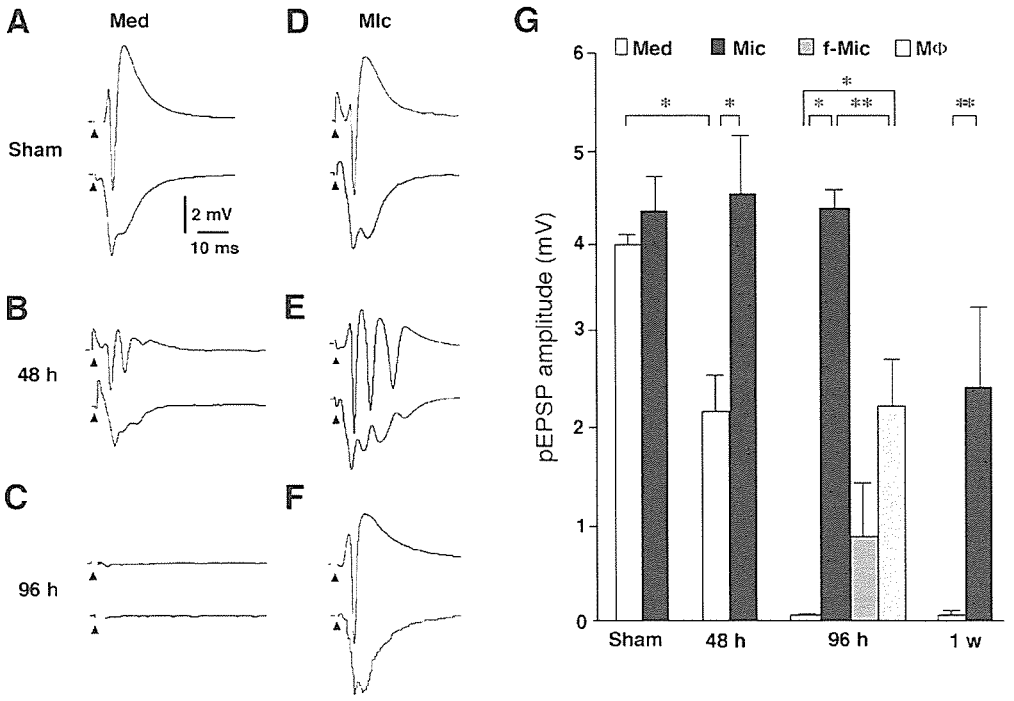

Fig. 2. Effects of the intra-arterial injection of microglia on the ischemia-induced changes of the synaptic field potentials in the hippocampal CA1 subfield. (A–C) Somatic (upper traces) and dendritic responses (lower traces) recorded simultaneously at various times after ischemia in the hippocampus prepared from medium (Med) -injected rats. (D–F) Somatic (upper traces) and dendritic responses (lower traces) recorded simultaneously at various times after ischemia in the hippocampus prepared from microglia (Mic) -injected rats. (A, D) Sham, (B, E) 48 h after ischemia, (C, F) 96 h after ischemia. These responses were evoked by the supra-maximal stimulation of Schaffer collateral afferents. The arrowheads indicate the onset of stimulation of the Schaffer collateral pathway. (G) The mean pEPSP amplitude in the CA1 subfield of hippocampal slices prepared from the Med-, Mic-, fixed-microglia- (f-Mic), or macrophage (Mϕ) -injected rats subjected to ischemia. Each column and vertical bar represents the mean and S.E. of 30 slices from five animals (Sam), 30 slices from five animals (48 h), 32 slices from five animals (96 h), 12 slices from three animals (1 w), 11 slices from three animals (f-Mic), 32 slices from five animals (Mϕ). Asterisks indicate a significant difference between the values (* $P<0.05$, ** $P<0.01$).

imal amplitude of pEPSP was significantly diminished compared with sham-operated control (Fig. 2B, G). In contrast, a pronounced hyperexcitability was observed in the hippocampal slices prepared from the microglia-injected animals at this stage. As shown in Fig. 2E, the synaptic field responses were characterized by multiple peaks. Furthermore, there was no significant change in the mean maximal amplitude of pEPSP recorded from the hippocampal slices subjected ischemia 48 h earlier as compared with sham-operated control (Fig. 2G). At 96 h after ischemia, no synaptic field potential was observed in the CA1 subfield of slices prepared from the medium-injected animals, while a presynaptic fiber volley was present (Fig. 2C). In the CA1 subfield of hippocampal slices prepared from the microglia-injected animals, rather normal responses were observed (Fig. 2F). In the microglia-injected animals, the synaptic field potentials of CA3–CA1 synapses were well preserved for up to 1 week (Fig. 2G). When the microglia fixed with 4% paraformaldehyde were injected intra-arterially, the pEPSP amplitude significantly decreased after ischemia (Fig. 2G). Intra-arterial injection of peripheral macrophages also showed a neuroprotective effect, while the mean restored amplitude of pEPSP of CA3–CA1 synapses by intra-arterial injection of microglia was on average 1.9-fold larger than that of intra-arterial injection of macrophage (Fig. 2G).

Protective effects of intra-arterial microglial injection against the ischemia-induced impairment of the efficacy of synaptic transmission

We have further examined the basal synaptic transmission and plasticity in the CA3–CA1 Schaffer collateral pathway of the medium- and microglia-injected animals subjected to ischemia 48 h earlier. We first constructed the input-output (I–O) relationships by plotting the mean pEPSP slope against the stimulus intensity. As shown in Fig. 3A, the mean pEPSP slope of the medium-injected animals stayed at a low level and it did not increase even after stronger stimulus intensities. On the other hand, no significant deficit in the I–O relationships was observed in the CA3–CA1 synapses of the microglia-injected animals (Fig. 3A). The mean maximal pEPSP slope of the microglia-injected animals was significantly larger than that of the medium-injected animals. Next, the I–O relationships were constructed by plotting the mean amplitude of the presynaptic fiber volley against the stimulus intensity. As shown in Fig. 3D, there was no significant difference between I–O curves of these two groups, thus indicating that the excitability of

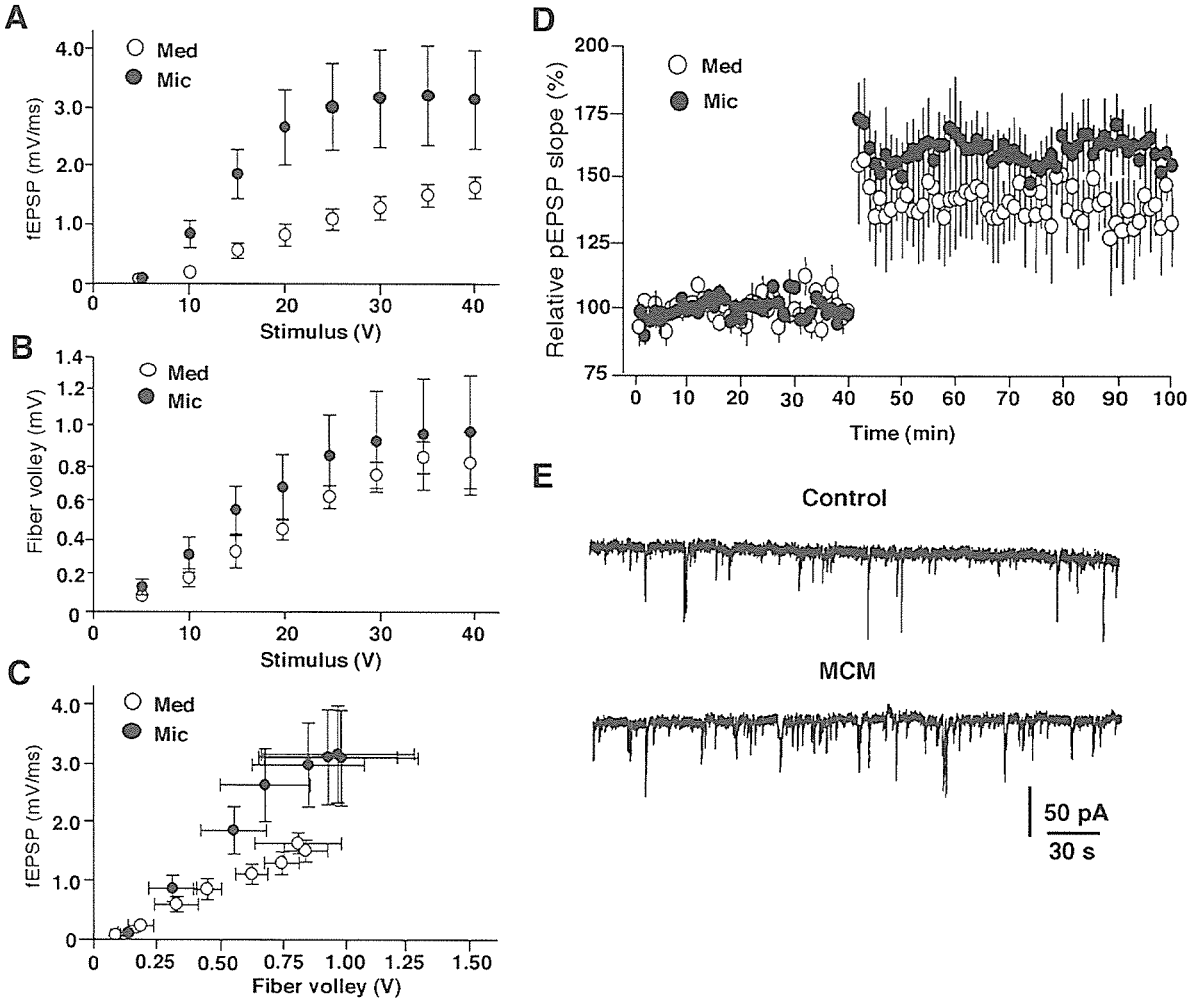

Fig. 3. (A–D) The effects of the intra-arterial injection of microglia on synaptic efficacy and LTP in the post-ischemic hippocampal CA1 subfield. (A–C) I–O relationships in the Schaffer collateral–CA1 synapses from the medium- (open circles) and microglia-injected animals (filled circles) subjected to ischemia 48 h earlier. (A) The mean pEPSP slope plotted against the stimulus intensity, (B) the mean amplitude of fiber volley plotted against the stimulus intensity, (C) the mean pEPSP slope plotted against the mean amplitude of fiber volley. (D) Relative pEPSP slope before and after tetanic stimulation (100 Hz, 1 s) in the CA3–CA1 synapses from the medium- and microglia-injected animals subjected to ischemia 48 h earlier. Each circle and bar represents mean and S.E. of three to five slices from three animals. (E) Effect of 10% MCM on spontaneous postsynaptic currents at a holding potential of −60 mV.

presynaptic fibers was not significantly affected by ischemia. When the I–O relationships were constructed by plotting the mean pEPSP slope against the mean amplitude of the presynaptic fiber volley, the mean slope of I–O curve of the microglia-injected rats (3.12±0.83 V/s, three slices from three animals) was significantly larger than that of the medium-injected rats (1.62±0.19 V/s, five slices from three animals) ($P<0.05$). Next, we also examined the formation of short-term synaptic plasticity and LTP in these two groups subjected to ischemia 48 h earlier. In both groups, there was no difference in paired-pulse facilitation between the medium- and microglia-injected animals (data not shown). As shown in Fig. 3D, the mean magnitude of LTP in the hippocampal slices prepared from the microglia-injected animals (159.4±7.7%, three slices from three animals) was larger than that from the medium-injected animals (136.4±13.5%, four slices from three animals). However, the difference did not reach statistical significance. These observations indicated that the ischemia-induced deficit in basal synaptic transmission and LTP in the CA3–CA1 synapses was markedly ameliorated by the arterial-injection of microglia.

To evaluate the possible effect of microglial diffusible factor(s) on presynaptic events, we further examined effects of MCM on spontaneous postsynaptic currents of CA1 neurons in hippocampal slices. As shown in Fig. 3E, the frequency of miniature response was significantly increased by 10% MCM. As shown in Fig. 3E, 10% MCM significantly increased the frequency of spontaneous postsynaptic currents by 130.5±15.4% of the control frequency ($P<0.05$, number of slices=4) without affecting the mean amplitude of the miniature responses. On the other hand, the 10% culture medium had no significant effect

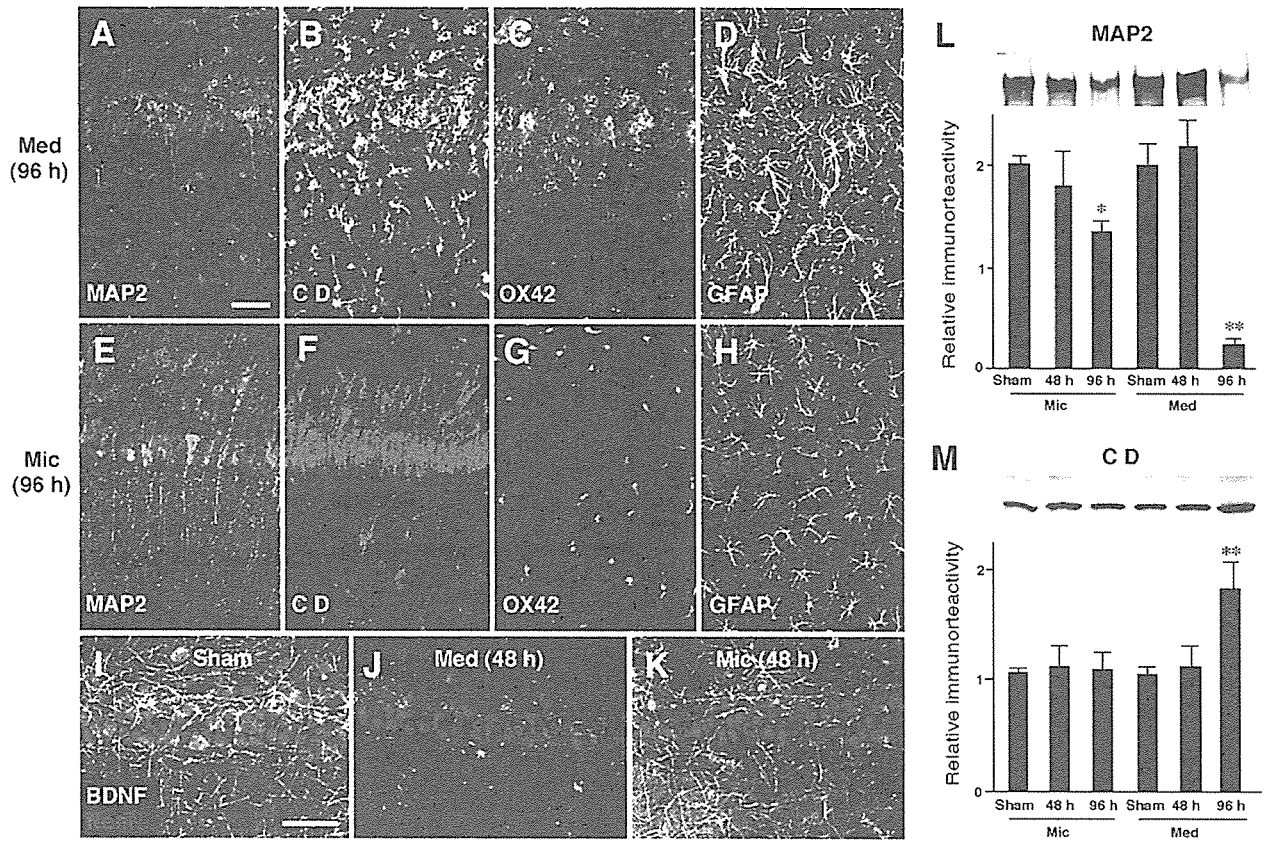

Fig. 4. Inhibition of ischemia-induced neurodegeneration and gliosis in the hippocampal CA1 subfield by the intra-arterial injection of microglia. (A–H) Immunofluorescent CLSM images (green) for MAP2 (A, E), CD (B, F), OX42 (C, G) and GFAP (D, H). (A–D) The hippocampus prepared from the medium (Med) -injected rats subjected to ischemia 96 h earlier. (E–H) The hippocampus prepared from the microglia (Mic) -injected rats subjected to ischemia 96 h earlier. The nuclei were stained by PI (red). Scale bar=100 μm. (I–K) Immunofluorescent double-labeled CLSM images for BDNF (green) and NeuN (red) in the hippocampal CA1 subfield. Sham: sham-operated rats, 48h (Med): Med-injected rat subjected to ischemia 48 h earlier, 48 h (Mic): Mic-injected rat subjected to ischemia 48 h earlier. Scale bar=50 μm. (L, M) Immunoblot analyses of the extracts of the hippocampus prepared from the Mic- and Med-injected rats subjected to ischemia by anti-MAP2 (L) or anti-CD antibody (M). Mic: hippocampal extracts prepared from the Mic-injected rats, Med: hippocampal extracts prepared from the Med-injected rats. Sham: sham-operated rats, 48 h: rat subjected to ischemia 48 h before, 96 h: rat subjected to ischemia 96 h before. Asterisks indicate a significant difference from the value obtained in the Sham rats (* $P<0.05$, ** $P<0.01$).

(97.3±4.2% of the control frequency, number of slices=4) (data not shown).

Effects of the intra-arterial microglial injection on the ischemia-induced neuronal death and gliosis in the hippocampal CA1 subfield

In the hippocampal sections prepared from the medium-injected animals subjected to ischemia 96 h earlier, marked neuronal degeneration and gliosis were obvious in the CA1 subfield as evidenced by condensed PI-stained nuclei of CA1 neurons and marked decrease in the immunoreactivity for MAP2 (Fig. 4A). It was also noted that the reduction of MAP2-immunorectivity was restricted in the CA1 subfield. Furthermore, GFAP and OX42-positive cells, which had thick processes, were frequently found in the CA1 subfield, indicating the formation of gliosis (Fig. 4C, D). The immunoreactivity for CD also markedly increased in the CA1 subfield (Fig. 4B). The increased immunoreactivity for CD is considered to mainly reflect gliosis due to neurodegeneration as previously reported (Nakanishi et al., 1993, 1994). Therefore, it is likely that the total loss of postsynaptic field potentials at this stage is due to an irreversible state of impairment. In contrast, we could not detect any significant loss of MAP2 immunoreactivity or a significant increase in CD immunoreactivity in the CA1 subfield of the hippocampal sections prepared from the microglia-injected animals subjected ischemia 96 h earlier (Fig. 4E, F). Furthermore, the signs for cellular activation of glial cells including morphological transformation and cell proliferation were barely detected in the CA1 subfield of these animals (Fig. 4G, H).

Immunohistological observations were further substantiated by immunoblot analyses. In the hippocampal extracts prepared from the medium-injected animals subjected to ischemia 96 h earlier, MAP2 level was significantly decreased (Fig. 4L). The mean amount of MAP2 was approximately 15% of that obtained from sham animals. In the hippocampal extracts prepared from the microglia-injected animals subjected to ischemia 96 h earlier, the level of MAP2 was markedly restored. The mean

amount of MAP2 was approximately 70% of that obtained from sham animals. On the other hand, the mean amount of CD significantly increased in the hippocampal extracts prepared from the medium-injected animals subjected to ischemia 96 h earlier (Fig. 4M). The increased immunoreactivity for CD is considered to mainly reflect gliosis due to neurodegeneration as reported previously (Nakanishi et al., 1993, 1994). In contrast, there was no significant change in the mean amount of CD in the postischemic hippocampus taken from the microglia-injected animals.

Finally, we examined the levels of BDNF immunoreactivity in the postischemic hippocampus taken from the medium- and microglia-injected animals subjected to ischemia, because the exogenously migrated microglia enhanced the BDNF level in neighboring neurons (Suzuki et al., 2001). In the sham animals, the intense immunoreactivities of BDNF were mainly found in the somata and dendrites of CA1 neurons (Fig. 4I). At 48 h after ischemia, the immunoreactivity of the BDNF in CA1 neurons of the medium-injected rats was markedly decreased (Fig. 4J). On the other hand, the immunoreactivity of BDNF in CA1 neuron of the microglia-injected animals remained well preserved (Fig. 4K). The mean level of intensity of BDNF immunofluorescence in the CA1 subfield of the ischemic hippocampus prepared from microglia-injected animals was on average 3.1-fold higher than from medium-injected animals (number of animals=3, $P<0.01$).

DISCUSSION

The major finding of the present study is that the intra-arterial injection of immortalized microglial cells, GMIR1, significantly ameliorated the ischemia-induced functional and morphological changes of hippocampal CA1 neurons in rats. In the hippocampal slices prepared from the medium-injected rats subjected to ischemia 48 h earlier, the evoked synaptic responses in the CA1 subfield became diminished without significant changes in levels of either MAP2 or CD. Our observations here are consistent with previous reports that the synaptic activity and plasticity both significantly decreased after ischemia (Urban et al., 1989; Hori and Carpenter, 1994; Kirino et al., 1992; Xu and Pulsinelli, 1994, 1996; Shinno et al., 1997). At 96 h after ischemia, the evoked synaptic responses in the CA1 subfield totally disappeared. At this stage, we found a significant decrease in the MAP2 level and a significant increase in the CD level in the hippocampus. Therefore, the decreased amplitude of evoked synaptic responses at 48 h after ischemia is most likely due to a dysfunction in the transmission rather than an irreversible state of impairment (Shinno et al., 1997; Zhang et al., 1999). On the other hand, the total loss of the postsynaptic field potentials at 96 h after ischemia is considered to reflect an irreversible state of impairment (Urban et al., 1989). In the present study, we found that the intra-arterial injection of microglia significantly protected the CA1 neurons against the ischemia-induced deficit in basal synaptic transmission and LTP in the CA3–CA1 glutamatergic synapses. The intra-arterial injection of microglia also inhibited the ischemia-induced neuronal degeneration and resultant gliosis in the CA1 subfield. The neuroprotective effect of intra-arterial-injected microglia was not observed by the fixation of microglia before injection. Therefore, the protective effect of intra-arterial-injected microglia on CA1 neurons against ischemic neuronal damage is considered to be due to the direct effect of infiltrated microglia rather than by indirect effects such as an incomplete reduction of the rCBF or hypothermia caused by the injection of microglia during occlusion. In the present study, approximately 2000 cells of exogenous microglia were found to migrate to the hippocampus after intra-arterial injection of 2×10^6 cells. This is consistent with the observations reported by Kitamura et al. (2004) that neuroprotective effect of i.c.v.-injected 4000 cells of microglia was equal to or may be higher than that of the 40,000 cells of microglia. Therefore, it is reasonable to consider that approximately 2000 of the microglial cells at the pathological site were sufficient to exert neuroprotection against ischemic neuronal damage.

Transient forebrain ischemia causes a complex cellular response that leads to the delayed neuronal death of specific neuronal populations in both humans and animal models (Pulsinelli et al., 1982; Kirino, 1982; Zola-Morgan et al., 1986, 1992). Even though extensive studies have been performed, the delayed nature of neuronal death of hippocampal CA1 neurons is still not fully understood. Shinno et al. (1997) have demonstrated that the reduction of the synaptic transmission in CA1 neurons in the early phase of ischemic insult may cause disruption of neurotrophic supply, thus leading to the apoptotic process. There is accumulating evidence that the ischemia-induced synaptic dysfunction may result from a low probability of transmitter release. Zhang et al. (1999) have reported that the amplitude of population spikes evoked in the CA1 subfield of hippocampal slices prepared from the post-ischemic rats was significantly restored by 4-aminopyridine, which is known to enhance transmitter release probability. More recently, it has been reported that ischemia-like condition (anoxia and aglycemia) significantly reduced the mean frequency of miniature excitatory postsynaptic currents recorded from CA1 neurons without affecting the amplitude (Tanaka et al., 2001). It has been recognized that the neuronal activity and neurotrophic factors interact reciprocally. The blockade of synaptic activities with TTX inhibits production and release of BDNF (Castrén et al., 1992), whereas glutamate stimulates BDNF production and release (Zafra et al., 1991). Furthermore, both mRNA and protein levels of BDNF were significantly decreased in the hippocampus after ischemia (Kokaia et al., 1996; Lee et al., 2002). Our observations herein showed that the intra-arterial injection of microglia prevented the ischemia-induced reduction of the BDNF levels in CA1 neurons. In the present study, we also found that MCM significantly increased the frequency of spontaneous postsynaptic currents of CA1 neurons without affecting the amplitude, thus indicating that MCM increased the provability of the neurotransmitter release. Therefore, it is tempting to speculate that the exogenously migrated microglia in the hippocampus ameliorated the ischemia-induced synaptic hypoactiv-

ity by the release of diffusible factor(s) that may increase the release of glutamate. The intra-arterial injection of microglia then preserved the BDNF levels, thus protecting CA1 neurons against the ischemia-induced neuronal degeneration. Furthermore, we recently reported that microglia secrete soluble factors that facilitate *N*-methyl-D-aspartic acid (NMDA) receptor-mediated glutamatergic neurotransmission (Moriguchi et al., 2003; Hayashi et al., 2006). These diffusible factors released by the exogenously migrated microglia may also contribute to the increased expression of BDNF because the activation of synaptic NMDA receptors has been shown to increase the expression level of BDNF (Hardingham et al., 2002). Additional experiments are necessary to identify the microglial diffusible factor(s) that could ameliorate the ischemia-induced synaptic deficits.

CONCLUSION

In conclusion, the arterial-injection of microglia protected against the ischemia-induced neuronal degeneration in the hippocampus possibly through the restoration of basal glutamatergic transmission and BDNF levels. Therefore, the arterial-injection of microglia might thus be a potentially effective therapeutic modality for the treatment of acute brain injury including cerebral ischemia.

Acknowledgments—This study was supported by Grants-in-Aid for the Creation of Innovations through Business-Academic-Public Sector Cooperation of Japan, and Grants-in-Aid for Scientific Research on Priority Area (No.15082204) from the Ministry of Education, Science and Culture, Japan.

REFERENCES

Castrén E, Zafra F, Thoenen H, Lindholm D (1992) Light regulates expression of brain-derived neurotrophic factor mRNA in rat visual cortex. Proc Natl Acad Sci U S A 89:9444–9448.

Hardingham GE, Fukunaga Y, Bading H (2002) Extrasynaptic NMDARs oppose synaptic NMDARs by triggering CREB shut-off and cell death pathways. Nat Neurosci 5:405–414.

Hayashi Y, Ishibashi H, Hashimoto K, Nakanishi H (2006) Potentiation of the NMDA receptor-mediated responses through the activation of the glycine site by microglia secreting soluble factors. Glia 53:660–668.

Hori N, Carpenter DO (1994) Functional and morphological changes induced by transient in vivo ischemia. Exp Neurol 129:279–289.

Imai F, Sawada M, Suzuki H, Kiya N, Hayakawa M, Nagatsu T, Marunouchi T, Kanno T (1997) Migration activity of microglia and macrophages into rat brain. Neurosci Lett 237:49–52.

Imai F, Sawada M, Suzuki H, Zlokovic BV, Kojima J, Kuno S, Nagatsu T, Nitatori T, Uchiyama Y, Kanno T (1999) Exogenous microglia enter the brain and migrate into ischaemic hippocampal lesions. Neurosci Lett 272:127–130.

Imai Y, Ibata I, Ito D, Ohsawa K, Kohsaka S (1996) A novel gene iba1 in the major histocompatibility complex class III region encoding an EF hand protein expressed in a monocytic lineage. Biophys Biochem Res Commun 224:855–862.

Kirino T (1982) Delayed neuronal death in the gerbil hippocampus following ischemia. Brain Res 239:57–69.

Kirino T, Robinson HPC, Miwa A, Tamura A, Kawai N (1992) Disturbance of membrane function preceding ischemic delayed neuronal death in the gerbil hippocampus. J Cereb Blood Flow Metab 12:408–417.

Kitamura Y, Takata K, Inden M, Tsuchiya D, Yanagisawa D, Nakata J, Taniguchi T (2004) Intraventricular injection of microglia protects against focal brain ischemia. J Pharmacol Sci 94:203–206.

Kitamura Y, Yanagisawa D, Inden M, Takata K, Tsuchiya D, Kawasaki T, Taniguchi T, Shimohama S (2005) Recovery of focal brain ischemia-induced behavioral dysfunction by intracerebroventricular injection of microglia. J Pharmacol Sci 97:289–293.

Kokaia Z, Nawa H, Uchino H, Elmér E, Kokaia M, Carnahan J, Smith ML, Siesjö BK, Lindvall O (1996) Regional brain-derived neurotrophic factor mRNA and protein levels following transient forebrain ischemia in the rat. Mol Brain Res 38:139–144.

Lee TH, Kato H, Chen ST, Kogre K, Itoyama Y (2002) Expression disparity of brain-derived neurotrophic factor immunoreactivity and mRNA in ischemic hippocampal neurons. Neuroreport 13: 2271–2275.

Lees GJ (1993) The possible contribution of microglia and macrophages to delayed neuronal death after ischemia. J Neurol Sci 114:119–122.

Liu J, Bartels M, Lu A, Sharp FR (2001) Microglia/macrophages proliferate in striatum and neocortex but not in hippocampus after brief global ischemia that produces ischemic tolerance in gerbil brain. J Cereb Blood Flow Metab 21:361–373.

Moriguchi S, Mizoguchi Y, Tomimatsu Y, Hayashi Y, Kadowaki T, Kagamiishi Y, Katsube N, Yamamoto K, Inoue K, Watanabe S, Nabekura J, Nakanishi H (2003) Potentiation of NMDA receptor-mediated synaptic responses by microglia. Mol Brain Res 119: 160–169.

Morihata H, Kawasaki J, Sakai H, Sawada M, Tsutada T, Kuno M (2000) Temporal fluctuations of voltage-gated proton currents in rat spinal microglia via pH- dependent and -independent mechanisms. Neurosci Res 38:265–271.

Nakanishi H, Tsukuba T, Kondou T, Tanaka T, Yamamoto K (1993) Transient forebrain ischemia induces expression and specific localization of cathepsins E and D in rat hippocampus and neostriatum. Exp Neurol 121:215–223.

Nakanishi H, Tominaga K, Amano T, Yamamoto K (1994) Age-related changes in activities and localizations of cathepsins D, E, B and L in the rat brain tissues. Exp Neurol 126:119–128.

Pulsinelli WA, Brierley JB (1979) A new model of bilateral hemispheric ischemia in the unanesthetized rat. Stroke 10:267–272.

Pulsinelli WA, Brierley JB, Plum F (1982) Temporal profile of neuronal damage in a model of transient forebrain ischemia. Ann Neurol 11:491–498.

Salimi K, Moser K, Zassler B, Reindl M, Embacher N, Schermer C, Wes C, Marksteiner J, Sawada M, Humpel C (2002) Glial cell line-derived neurotrophic factor enhances survival of GM-CSF dependent rat GMIR1-microglial cells. Neurosci Res 43:221–229.

Sawada M, Imai F, Suzuki H, Hayakawa M, Kanno T, Nagatsu T (1998) Brain-specific gene expression by immortalized microglial cell-mediated gene transfer in the mammalian brain. FEBS Lett 433:37–40.

Shimizu T, Hayashi Y, Yamasaki R, Yamada J, Zhang J, Ukai K, Koike M, Mine K, von Figura K, Peters C, Saftig P, Fukuda T, Uchiyama Y, Nakanishi H (2005) Proteolytic degradation of glutamate decarboxylase mediates disinhibition of hippocampal CA3 pyramidal cells in cathepsin D-deficient mice. J Neurochem 94:680–690.

Shinno K, Zhang L, Eubanka JH, Carlen PL, Wallance MC (1997) Transient ischemia induces an early decrease of synaptic transmission in CA1 neurons of rat hippocampus: electrophysiologic study in brain slices. J Cereb Blood Flow Metab 17:955–966.

Suzuki H, Imai F, Kanno T, Sawada M (2001) Preservation of neurotrophin expression in microglia that migrate into the gerbil's brain across the blood-brain barrier. Neurosci Lett 312:95–98.

Tanaka E, Yasumoto S, Hattori G, Niyama S, Matsuyama S, Higashi H (2001) Mechanism underlying the depression of evoked fast EPSCs following in vitro ischemia in rat hippocampal CA1 neurons. J Neurophysiol 86:1095–1103.

Tomimatsu Y, Idemoto K, Moriguchi S, Watanabe S, Nakanishi H (2002) Proteases involved in long-term potentiation. Life Sci 72:355–361.

Urban L, Neill KH, Crain BJ, Nadler JV, Somjen GG (1989) Postischemic synaptic physiology in area CA1 of the gerbil hippocampus studied in vitro. J Neurosci 9:3966–3975.

Xu ZC, Pulsinelli WA (1994) Responses of CA1 pyramidal neurons in rat hippocampus to transient forebrain ischemia: an in vivo intracellular recording study. Neurosci Lett 171:187–191.

Xu ZC, Pulsinelli WA (1996) Electrophysiological changes of CA1 pyramidal neurons following transient forebrain ischemia: an in vivo intracellular recording and staining study. J Neurophysiol 76: 1689–1697.

Yrjänheikki J, Keinänen R, Pellikka M, Hökfelt T, Koistinaho J (1998) Tetracyclines inhibit microglial activation and are neuroprotective in global brain ischemia. Proc Natl Acad Sci U S A 95:15769–15774.

Zafra F, Castrén E, Thoenen H, Lindholm D (1991) Interplay between glutamate and γ-aminobutyric acid transmitter systems in the physiological regulation of brain-derived neurotrophic factor and nerve growth factor synthesis in hippocampal neurons. Proc Natl Acad Sci U S A 88:10037–10041.

Zhang L, Shang Y, Tian GF, Wallance MC, Eubanks JH (1999) Reversible attenuation of glutamatergic transmission in hippocampal CA1 neurons of rat brain slices following transient cerebral ischemia. Brain Res 832:31–39.

Zola-Morgan S, Squire LR, Amaral DG (1986) Human amnesia and the media temporal region: enduring memory impairment following a bilateral lesion limited to field of the hippocampus. J Neurosci 6:1967–2950.

Zola-Morgan S, Squire LR, Rempel NL, Clower PR, Amaral DG (1992) Enduring memory impairment in monkeys after ischemic damage to the hippocampus. J Neurosci 12:2582–2596.

(Accepted 2 June 2006)
(Available online 14 July 2006)

Available online at www.sciencedirect.com
ScienceDirect
Biochemical and Biophysical Research Communications 349 (2006) 913–919
BBRC
www.elsevier.com/locate/ybbrc

Cell cycle-dependent regulation of kainate-induced inward currents in microglia

Jun Yamada [a], Makoto Sawada [b], Hiroshi Nakanishi [a,*]

[a] *Laboratory of Oral Aging Science, Faculty of Dental Sciences, Kyushu University, Fukuoka 812-8582, Japan*
[b] *Department of Brain Life Science, Research Institute of Environmental Medicine, Nagoya University, Nagoya 464-8601, Japan*

Received 8 August 2006
Available online 31 August 2006

Abstract

Microglia are reported to have α-amino-hydroxy-5-methyl-isoxazole-4-propionate/kainate (KA) types. However, only small population of primary cultured rat microglia (approximately 20%) responded to KA. In the present study, we have attempted to elucidate the regulatory mechanism of responsiveness to KA in GMIR1 rat microglial cell line. When the GMIR1 cells were plated at a low density in the presence of granulocyte macrophage colony-stimulating factor, the proliferation rate increased and reached the peak after 2 days in culture and then gradually decreased because of density-dependent inhibition. At cell proliferation stage, approximately 80% of the GMIR1 cells exhibited glutamate (Glu)- and KA-induced inward currents at cell proliferation stage, whereas only 22.5% of the cells showed responsiveness to Glu and KA at cell quiescent stage. Furthermore, the mean amplitudes of inward currents induced by Glu and KA at cell proliferation stage (13.8 ± 3.0 and 8.4 ± 0.6 pA) were significantly larger than those obtained at cell quiescent stage (4.7 ± 0.8 and 6.2 ± 1.2 pA). In the GMIR1 cells, KA-induced inward currents were markedly inhibited by (*RS*)-3-(2-carboxybenzyl) willardiine (UBP296), a selective antagonist for KA receptors. The KA-responsive cells also responded to (*RS*)-2-amino-3-(3-hydroxy-5-*tert*-butylisoxazol-4-yl) propanoic acid (ATPA), a selective agonist for GluR5, in both GMIR1 cells and primary cultured rat microglia. Furthermore, mRNA levels of the KA receptor subunits, GluR5 and GluR6, at the cell proliferation stage were significantly higher than those at the cell quiescent stage. Furthermore, the immunoreactivity for GluR6/7 was found to increase in activated microglia in the post-ischemic hippocampus. These results strongly suggest that microglia have functional KA receptors mainly consisting of GluR5 and GluR6, and the expression levels of these subunits are closely regulated by the cell cycle mechanism.

Keywords: Microglia; Kainate; Granulocyte–macrophage colony-stimulating factor; Whole-cell patch clamp; Real-time quantitative RT-PCR

There is increasing evidence that glutamate (Glu) is one of the important molecules mediating the neuron-to-microglia communication in both physiological and pathological states [1–5]. We have previously reported that microglia express functional ionotropic Glu receptors, mainly α-amino-hydroxy-5-methyl-isoxazole-4-propionate (AMPA)/kainate (KA) types. Although the activation of these receptors enhanced the release of proinflammatory cytokines including tumor necrosis factor-α, only 20% of the primary cultured rat microglia could elicit inward currents after the application of KA [5]. However, the reason why the KA-responsive population of the microglia is so small. Gottlieb and Matute [6] have reported that the levels of Glu receptor subunits expressed in the microglia peaked between 3 and 7 days after transient forebrain ischemia, a time when strong microglial activation and proliferation were observed in the CA1 subfield of the hippocampus [7]. Furthermore, it is also known that a marked expression of cyclin D1, a key regulator of cell cycle progression, was followed by microglial proliferation [7,8]. This may suggest that the expression of Glu receptors in the microglia is closely linked with the cell cycle. To investigate this

* Corresponding author. Fax: +81 92 642 6415.
E-mail address: nakan@dent.kyushu-u.ac.jp (H. Nakanishi).

0006-291X/$ - see front matter © 2006 Elsevier Inc. All rights reserved.
doi:10.1016/j.bbrc.2006.08.126